Temporally resolved early BMP-driven transcriptional cascade during human amnion specification

AUTHORS:
Nikola Sekulovski[1], Jenna C. Wettstein[1], Amber E. Carleton[1], Linnea E. Taniguchi[1], Xiaolong Ma[2], Sridhar Rao[1,3,4], Jenna K. Schmidt[5], Thaddeus G. Golos[5,6,7], Chien-Wei Lin[2, †] and Kenichiro Taniguchi[1,3,†]

AFFILIATIONS:
[1]Department of Cell Biology, Neurobiology and Anatomy, Medical College of Wisconsin, Milwaukee, WI 53226, USA
[2]Division of Biostatistics, Institute for Health and Equity, Medical College of Wisconsin, Milwaukee, WI 53226, USA
[3]Department of Pediatrics, Medical College of Wisconsin, Milwaukee, WI 53226, USA
[4]Versiti Blood Research Institute, Milwaukee, WI 53226 USA
[5]Wisconsin National Primate Research Center (WNPRC), Madison, WI, USA
[6]Department of Obstetrics and Gynecology, University of Wisconsin - Madison School of Medicine and Public Health, Madison, WI USA
[7]Department of Comparative Biosciences, University of Wisconsin - Madison School of Veterinary Medicine, Madison, WI, USA

[†]Co-corresponding authors

CONTACT:

Kenichiro Taniguchi
8701 Watertown Plank Road
B4245 BSB CB062
Milwaukee, WI 53226
ktaniguchi@mcw.edu

Chien-Wei Lin
8701 Watertown Plank Road
MEB M1406
Milwaukee, WI 53226
chlin@mcw.edu

ABSTRACT

Amniogenesis, a process critical for continuation of healthy pregnancy, is triggered in a collection of pluripotent epiblast cells as the human embryo implants. Previous studies have established that BMP signaling is a major driver of this lineage specifying process, but the downstream BMP-dependent transcriptional networks that lead to successful amniogenesis remain to be identified. This is, in part, due to the current lack of a robust and reproducible model system that enables mechanistic investigations exclusively into amniogenesis. Here, we developed an improved model of early amnion specification, using a human pluripotent stem cell-based platform in which the activation of BMP signaling is controlled and synchronous. Uniform amniogenesis is seen within 48 hours after BMP activation, and the resulting cells share transcriptomic characteristics with amnion cells of a gastrulating human embryo. Using detailed time-course transcriptomic analyses, we established a previously uncharacterized BMP-dependent amniotic transcriptional cascade, and identified markers that represent five distinct stages of amnion fate specification; the expression of selected markers was validated in early post-implantation macaque embryos. Moreover, a cohort of factors that could potentially control specific stages of amniogenesis was identified, including the transcription factor TFAP2A. Functionally, we determined that, once amniogenesis is triggered by the BMP pathway, TFAP2A controls the progression of amniogenesis. This work presents a temporally resolved transcriptomic resource for several previously uncharacterized amniogenesis states and demonstrates a critical intermediate role for TFAP2A during amnion fate specification.

INTRODUCTION

The amniotic epithelium is the innermost layer of the amniochorionic membrane that physically divides the maternal and fetal environments (Miki et al., 2005; Miki and Strom, 2006). Amniogenesis is initiated during implantation in humans (and in non-human primates), eventually leading to the formation of an amniotic sac structure that surrounds and protects the developing embryo (Enders et al., 1983; Enders et al., 1986; Miki et al., 2005; Sasaki et al., 2016; Shahbazi and Zernicka-Goetz, 2018; Taniguchi et al., 2019). At implantation, the embryo (referred to at this time as a blastocyst) contains three functionally distinct cell types: a collection of unpolarized pluripotent epiblast cells (precursors to the embryo proper and amniotic ectoderm), a surrounding layer of polarized trophectoderm (a placental tissue precursor) and an underlying extraembryonic primitive endoderm (a yolk sac precursor). During implantation, the pluripotent epiblast cells undergo apico-basal polarization to form a cyst with a central lumen, the future amniotic cavity (Carleton et al., 2022). This event is followed by the fate transition of pluripotent epiblast cells at the uterine-proximal pole of the cyst to squamous amniotic ectoderm, forming a sharp boundary between amnion and pluripotent epiblast portions of the cyst (Shahbazi and Zernicka-Goetz, 2018; Shao and Fu, 2022; Taniguchi et al., 2019). This structure, the amniotic sac, represents the substrate for the next essential steps of embryonic development. Recent transcriptomic studies of early human and non-human primate embryos have presented benchmark resources for the amnion transcriptome of primates (Bergmann et al., 2022; Nakamura et al., 2016; Nakamura et al., 2017; Sasaki et al., 2016; Tyser et al., 2021; Yang et al., 2021).

77 The mechanistic dissection of human amnion development presents a challenge,
78 since it is ethically unacceptable to manipulate human embryos *in vivo* and technically
79 difficult to carry out such studies *in vitro*. Non-human primate (NHP) embryos such as
80 rhesus macaque are a suitable alternative to human embryos, due to their close
81 ancestral similarities (Nakamura et al., 2021), and have already provided crucial insights
82 into molecular processes that could potentially regulate amniogenesis. Indeed, genetic
83 manipulation has been demonstrated in NHP systems to study peri-implantation
84 embryogenesis (Yang et al., 2021), although this is not yet a widely applicable approach
85 due to resource availability and logistical complexity of such studies, which also carry
86 their own unique ethical challenges.

87 Previously, we developed an *in vitro* system of human amnion development
88 called Gel-3D (Shao et al., 2017a; Shao et al., 2017b), in which human pluripotent stem
89 cells (hPSC) are plated on a soft gel substrate consisting of extracellular matrix (ECM).
90 Within 24 hours, aggregates of hPSC form polarized cysts composed of columnar
91 pluripotent cells. Over the next three to four days, a 3D environment is introduced by
92 supplementing the culture medium with a diluted ECM overlay. Under these conditions,
93 the initially pluripotent cysts spontaneously undergo squamous morphogenesis, lose
94 pluripotency markers, and begin to express amnion markers; in over 90% of such cysts,
95 the central lumen becomes entirely surrounded by squamous amnion cells (hPSC-
96 amnion, (Shao et al., 2017a)). Using this system, we showed that mechanically
97 activated Bone Morphogenetic Protein (BMP) signaling can trigger amniogenesis and
98 identified several genes that are now used as amnion markers (e.g., GATA3, TFAP2A,
99 GABRP, (Shao et al., 2017a; Shao et al., 2017b)). These findings were supported by

later studies using early human embryo-like models as well as by single cell transcriptomic studies in early human and NHP embryos (Chen et al., 2021; Tyser et al., 2021; Yang et al., 2021; Zheng et al., 2019; Zheng et al., 2022).

Though this Gel-3D system (Shao et al., 2017a) has been valuable in allowing initial investigations of the mechanisms underlying amniogenic differentiation, it suffers from the fact that the initiation of amniogenesis by mechanical cues is stochastic and is not fully penetrant, hindering reproducible examinations into temporally and spatially sensitive processes. To better implement mechanistic studies, we developed a highly reproducible hPSC-based amniogenic system, called Glass-3D^{+BMP}, that does not rely on the mechanically activated spontaneous BMP signaling to initiate amniogenesis. Rather, in Glass-3D^{+BMP}, BMP4 ligand is added exogenously, and the amniotic differentiation response is quickly seen in all cells. Interestingly, while BMP signaling activation is immediately detectable in all cells, squamous morphogenesis (starting approximately 24 hours after BMP4 addition) is initially focal within a given cyst, but then spreads laterally, to form fully squamous amnion cysts by 48 hours. Such amnion cysts (hPSC-amnion) are uniformly composed of mature amniotic cells that share similar transcriptomes with amnion cells from a Carnegie stage (CS) 7 human embryo (dataset from (Tyser et al., 2021)).

Given the robust and synchronous nature of this system, we perform detailed time-course bulk RNA sequencing analyses of developing Glass-3D^{+BMP} hPSC-amnion to comprehensively characterize changes in transcriptional characteristics during the initial stages of amnion fate specification. Strikingly, from 0 to 48 hours after BMP treatment, developing hPSC-amnion displays transcriptomic characteristics of epiblast,

123 primitive streak-like or amnion cells that are present in the CS7 human embryo,
124 revealing a potential amnion differentiation trajectory. Moreover, we systematically
125 characterize dynamically expressed genes, and identify immediate-, early-,
126 intermediate- and late-responding genes associated with amniotic differentiation, some
127 of which are validated and characterized in detail in NHP embryos. Interestingly, in
128 contrast to the previous idea that TFAP2A is a *pan*-amnion marker expressed
129 throughout amniogenesis, we establish that TFAP2A is an early/intermediate
130 responding gene, with a temporal pattern of activation that is distinct from immediate
131 responding genes such as GATA3, another *pan*-amnion marker. Functional analyses
132 show that, in the absence of TFAP2A, amniogenesis is incomplete, suggesting that
133 TFAP2A controls amnion fate progression. Lastly, we identify a population of cells at the
134 boundary of the amnion and the epiblast in the peri-gastrula macaque embryo that
135 shares striking molecular and cellular characteristics of cells undergoing amnion
136 specification in Glass-3D^{+BMP}. Together, using the Glass-3D^{+BMP} amnion platform, these
137 studies present a transcriptomic map of the early stages of amnion differentiation, and
138 identify a critical transcriptional pathway dependent on TFAP2A, as well as a potential
139 site of active amniogenesis in the primate peri-gastrula.
140

141 **RESULTS**

142 **Generation of fully squamous hPSC-derived amniotic cysts in a reproducible and**
143 **controlled manner using a Glass-3D^{+BMP} culture system**

144 Targeted mechanistic investigations into amnion fate specification has been limited by
145 the fact that amniogenesis is not fully penetrant in existing *in vitro* embryo-like models

146 (Chen et al., 2021; Nasr Esfahani et al., 2019; Shao et al., 2017a; Shao et al., 2017b;
147 Zheng et al., 2019), prompting us to explore alternative strategies. Since our previous
148 studies have established that BMP signaling is a major driver of amniogenesis (Shao et
149 al., 2017a; Shao et al., 2017b), we sought to establish a system in which we could
150 directly control the activation of BMP signaling. We began with a culture condition called
151 Glass-3D, in which aggregates of hPSC are cultured in a stiff glass substrate condition
152 with the culture medium supplemented with a 3D ECM overlay (**Fig. 1A**). Under these
153 conditions, aggregates of hPSC initiate radial organization and form cysts with a central
154 lumen within 48 hours (Shao et al., 2017a; Taniguchi et al., 2017; Taniguchi et al.,
155 2015). Importantly, these cysts are composed entirely of polarized pluripotent cells.
156 When we examined the polarized membrane spatial proteomics of these hPSC-
157 pluripotent cysts, we found that BMP receptors are enriched at the basolateral
158 membrane territory (Wang et al., 2021). To test whether BMP signaling could be directly
159 activated in these cysts by the addition of BMP to the medium, pluripotent cysts (derived
160 from H9 (WA09) human embryonic stem cells for all experiments, unless otherwise
161 noted) were treated with exogenously provided BMP4 at d2 (**Fig. 1B**, Glass-3D^{+BMP}).
162 Nuclear localization of phosphorylated SMAD1/5 (pSMAD1/5), as detected by
163 immunofluorescence (IF), was used as a readout for BMP signaling activation (**Fig. 1C**).
164 At d2 in Glass-3D, prior to the addition of BMP, a polarized pluripotent (SOX2^{+}) cyst
165 structure has formed, and a small central lumen is visible (**Fig. 1C** – 0-min); this
166 structure is similar to that of the developing epiblast immediately prior to the initiation of
167 amniogenesis (Shahbazi and Zernicka-Goetz, 2018; Taniguchi et al., 2019). Strikingly,
168 within 10 minutes after BMP addition, uniform nuclear pSMAD1/5 enrichment is seen in

169 all treated cells at an equivalent level (**Fig. 1C** – 10-min, fluorescent quantitation in **Fig.**
170 **1D**). This is quickly followed by the expression of GATA3, a *pan*-amnion marker and a
171 well-known immediate downstream BMP target that has been shown to facilitate
172 pluripotency exit (Gunne-Braden et al., 2020). GATA3 expression is detected in all cells
173 within 3 hours (**Fig. 1E**), suggesting that BMP signaling is uniformly activated.
174 Interestingly, TFAP2A, another transcription factor thought to be an early *pan*-amnion
175 marker, is not detectable in GATA3 positive cells 3 hours after BMP addition (**Fig. 1E**).
176 After 48-hr of BMP4 treatment, all cysts show uniform squamous morphogenesis, loss
177 of pluripotency markers (NANOG, SOX2) and activated expression of additional *pan*-
178 amnion markers, TFAP2A and ISL1 (**Fig. 1F-H**).
179 To investigate whether exogenous BMP4 ligand is continuously needed
180 throughout the 48-hour time-course in order to form fully squamous hPSC-amnion, d2
181 pluripotent cysts were cultured with BMP4 for 24 hours (d2 to d3), then cultured without
182 BMP4 for the following 24 hours (d3 to d4), and then harvested at d4 (4 days after initial
183 plating, **Fig. 1B**). Interestingly, these 24-hr BMP treatment samples show fully
184 squamous amnion cysts that are morphologically and molecularly similar to those
185 treated over 48-hr. That is, they show uniformly squamous cyst morphogenesis and
186 prominent expression of GATA3, TFAP2A and ISL1, (**Fig. 1I,J**, quantitation for
187 fluorescent intensity and nuclear aspect ratios in **Fig. 1K,L**), as well as relatively similar
188 nuclear pSMAD1/5 signals (**Fig. 1M**). Moreover, in the 24-hr BMP treatment samples
189 (**Fig. 2A**), time-course analyses show that heterogeneous GATA3 expression is visible
190 in a few nuclei at 3-hr and 6-hr, becoming more prominent by 12-24-hr (**Fig. 2B-D**).
191 Early GATA3 expression is followed by initiation of TFAP2A expression by 12-hr (**Fig.**

192 **2B,D**). Two other "*pan*-amnion" genes, ISL1 and HAND1 become activated by 24-hr
193 (**Fig. 2C,E**), revealing a previously unrecognized GATA3 → TFAP2A → ISL1/HAND1
194 amniotic gene activation order (**Fig. 2B,C**, mRNA expression levels in **Fig. 2D,E**).
195 Importantly, SOX2 expression is abundant at 6-hr, fades in some nuclei at 12-hr and is
196 largely diminished by 24-hr (**Fig. 2B,C**, mRNA expression levels in **Fig. 2F**). NANOG
197 expression follows a similar time course to that of SOX2, revealing a gradual loss of
198 pluripotency (**Fig. 2F**). Samples treated with BMP4 for 24-hr or 48-hr display similar
199 levels of amnion and pluripotency markers (**Fig. 2G**), suggesting that BMP4 treatment
200 may be dispensable after the first 24 hours. To test this possibility, we treated cysts with
201 BMP4 for 24 hours (d2-d3) and subsequently treated with LDN-193189, a small
202 molecule inhibitor for the BMP receptor kinase activity (d3-d4). This treatment resulted
203 in fully squamous cysts that are positive for GATA3 and ISL1/2 (**Fig. 2H**), confirming
204 that BMP signaling initiates the early amniogenesis cascade, but is not required for its
205 progression.
206 Together, these results show that BMP4 treatment of d2 pluripotent cysts in a
207 Glass-3D culture environment provides a robust amniogenic model that enables
208 mechanistic investigations. We confirmed this finding in a human induced pluripotent
209 stem cell line (1196a, **Fig. S1**, (Chen et al., 2014)), further establishing this protocol as
210 an effective model of amnion fate conversion *in vitro*. Given that BMP4 treatment from
211 d3 to d4 is dispensable, 24-hour BMP4 treatment between d2 and d3 is used in all
212 remaining experiments using Glass-3D^{+BMP}, unless otherwise noted.
213
214 **Transcriptomic characterization of developing Glass-3D^{+BMP} hPSC-amnion**

215 To comprehensively understand the transcriptomic changes during hPSC-amnion
216 development in the Glass-3D^{+BMP} system, we performed bulk RNA sequencing analyses
217 for samples taken at 0-, 0.5-, 1-, 3-, 6-, 12-, 24- and 48-hr timepoints (post-BMP4
218 treatment). Samples were also taken from pluripotent monolayers and d4 pluripotent
219 cysts (**Fig. 3A** (experimental outline), **3B** (heatmap), **3C** (principal component analysis
220 (PCA)), see **Table 1A** for normalized and filtered counts). Overall, a total of 12,891
221 genes were detected among all sequenced samples. Similar to known immediate BMP-
222 responding genes (e.g., *ID2*, *BAMBI*), *GATA3* shows a significant increase by 1-hr, and
223 continuously increases overtime (**Fig. 3D**, >100-fold increase by 1-hr). Other markers
224 also display expected expression patterns (**Fig. 3E-G**). For example, *TFAP2A* and *ISL1*
225 show significant increases by 3-hr and 24-hr, respectively (**Fig. 3E**), and pluripotency
226 markers (**Fig. 3G**, *NANOG*, *OCT4/POU5F1*, *SOX2*) show reduction overtime. A
227 comparison of gene expression between d4 Glass-3D pluripotent cysts and d4 Glass-
228 3D^{+BMP} hPSC-amnion (48-hr timepoint) shows 1,820 upregulated and 2,092 down-
229 regulated (cut-off = 2-fold, $p<0.05$) genes in d4 Glass-3D^{+BMP} hPSC-amnion (**Fig. 3H**,
230 see **Table 1B,C** for full lists). Highly upregulated markers include known advanced
231 amnion state markers such as *GABRP*, *IGFBP3* and *EPAS1* (**Fig. 3H**), and highly
232 downregulated genes include *SOX2* and *NANOG* (**Fig. 3H**, see **Table 1D**,**E** for Gene
233 Ontology (GO) enrichment analyses (Biological Processes) for all significantly
234 upregulated and downregulated genes (> 2-fold, FDR < 0.05)).
235 The transcriptomic characteristics of developing amnion cells from a Carnegie
236 stage (CS) 7 human embryo were recently described by Tyser *et al.* (**Fig. 4A** shows a
237 UMAP (Uniform Manifold Approximation and Projection) plot with the original

238 coordinates and annotations, (Tyser et al., 2021)). In this analysis, the authors state that
239 yolk sac and connecting stalk tissues were discarded during dissection, but amnion
240 tissue was intact and included in the single cell preparation that was analyzed (Tyser et
241 al., 2021). Consistent with this notion, our analysis in which expression was
242 superimposed on the UMAP plot shows that *pan*-amnion markers such as *GATA3*,
243 *TFAP2A* and *ISL1* are broadly expressed in the rod-shaped cell population marked
244 "Ectoderm" (**Fig. 4B**, areas within the inset "**i**" are shown in **4B-D**; see **Fig. S2A** for
245 uncropped UMAP expression plots), suggesting that this region contains cells of the
246 amniotic lineage. We next examined which cells in the CS7 human embryo share
247 transcriptomic similarities to developing hPSC-amnion, and found that, indeed, the 48-hr
248 Glass-3D^{+BMP} samples exhibit clear transcriptional similarities to cells marked
249 "Ectoderm" in the CS7 human embryo (**Fig. 4C**), validating the human amnion-like
250 characteristics of our hPSC-amnion model. Interestingly, the earlier timepoints also
251 show overlaps with cell types of the CS7 human embryo (**Fig. 4C**, uncropped plot
252 shown in **Fig. S2B**). While pluripotent monolayer, d4 Glass-3D pluripotent cyst, as well
253 as 0-, 0.5-, 1-, 3- and 6-hr samples transcriptomically resemble Tyser "Epiblast" cells
254 (orange dots in **Fig. 4C**), 12-hr samples show transcriptomic similarities with cells
255 labeled in the Tyser analysis as "Primitive Streak"; these cells map close to the
256 Epiblast/Primitive Streak boundary in the Tyser UMAP (green dots in **Fig. 4C**). By 24-hr,
257 the transcriptomes are most similar to Tyser "Primitive Streak" cells proximal to the
258 amniotic "Ectoderm" (blue dots in **Fig. 4C**). Despite their "Primitive Streak" annotation,
259 these 24-hr cells adjacent to the amniotic "Ectoderm" population display relatively low
260 levels of *TBXT* (a major marker of primitive streak cells, **Fig. 4D**, (Beddington and

261 Robertson, 1999; Tyser et al., 2021; Zheng et al., 2019)), marking them as distinct from
262 the “Primitive Streak” cells progressing to “Nascent Mesoderm” (**Fig. 4D**). These
263 bioinformatic analyses suggest that the Glass-3D^{+BMP} amnion may develop from
264 pluripotent epiblast-like cells that are transcriptomically equivalent to the CS7 epiblast
265 cells, and, then traverse *TBXT*^{low} primitive streak-like intermediate states as the lineage
266 specification continues before acquiring an amniotic fate by 48-hr (dotted arrow, **Fig.**
267 **4C**).

268 Given that the hPSC-amnion differentiation trajectory in the Glass-3D^{+BMP} model
269 overlaps with cells in the CS7 human embryo, it appears that active amniogenesis
270 processes may be present in the early post-implantation embryo. Thus, we applied an
271 RNA velocity analysis (Bergen et al., 2020) to the Tyser data; in such an analysis,
272 lineage progression is inferred from comparing spliced and unspliced mRNA. **Fig. 5A**
273 (inset “**i**”) shows that the Tyser velocity data show differentiation trajectories very similar
274 to the one inferred from the time-course analysis of the Glass-3D^{+BMP} model
275 (trajectories starting from “Epiblast” → “Primitive Streak” → “Ectoderm”).

276 To further validate this notion in a primate system, we performed detailed IF
277 expression analyses for GATA3, TFAP2A, ISL1 and SOX2 in an early cynomolgus
278 macaque embryo staged between CS6 and CS7 (**Fig. 5B-E**). In this CS6/7 embryo, a
279 clear amniotic sac is seen, with SOX2^{+} epiblast cells on one side and contiguous ISL1^{+}
280 squamous amniotic ectoderm cells that are also positive for GATA3 and TFAP2A on the
281 other (**Fig. 5B-E**, fluorescent intensity quantitation shown in **5C,E**). Surface ectoderm
282 bridging neural ectoderm and amniotic ectoderm is not seen at this stage; this finding is
283 consistent with the previous histological studies in human (the Carnegie Collection,

284 found in the Virtual Human Embryo Project) and NHP pre- and peri-gastrula embryos
285 (Enders et al., 1983; Enders et al., 1986; Yang et al., 2021). Although amniotic
286 mesenchyme is not evident, some mesenchymal cells are observed underlying the
287 epiblast (**Fig. 5F**, green dotted bracket). These mesenchymal cells show abundant
288 nuclear pSMAD1/5: these cells are likely derived from the primitive streak (**Fig. 5F**).
289 Strikingly, at the boundary between the epiblast and amnion, a gradual transition in cell
290 morphology is readily seen: while cells most proximal to the epiblast are columnar, there
291 is a gradual reduction in height until fully squamous cells are seen (**Fig. 5B,D,F,H**),
292 represented by the changes in nuclear aspect ratio (**Fig. 5H**). Molecularly, the
293 expression of GATA3, TFAP2A, ISL1 and SOX2 is correlated with such columnar to
294 squamous cell shape change (**Fig. 5B-E**). While SOX2 expression shows a reducing
295 trend, the expression of GATA3, TFAP2A and ISL1 gradually increases in more distal
296 squamous cells (**Fig. 5B-E**, quantitation in **5C,E**). Furthermore, GATA3, TFAP2A and
297 ISL1 each display distinct expression patterns within the boundary cell population, as
298 the expression of GATA3 and TFAP2A is first detected in columnar $SOX2^{+}$ cells, but in
299 these cells, ISL1 is not observed (**Fig. 5C**). However, a weak but clear expression of
300 ISL1 can be found within ~10 distally located cells, from the first detected
301 $GATA3^{+}/TFAP2A^{+}$ cell. Similar observations are seen in another early cynomolgus
302 macaque embryo (**Fig. S3**, staged at CS7). This cell shape change associated with the
303 ordered transcriptional events (from GATA3, TFAP2A then ISL1) is similar to the
304 ordered morphological and molecular changes seen in developing Glass-$3D^{+BMP}$ hPSC-
305 amnion. Thus, the results based on these bioinformatic and expression analyses
306 provide evidence for the presence of amniotic fate progression in early post-gastrula

307 embryos at the boundary between amnion and epiblast (a schematic model shown in
308 **Fig. 5I**).
309
310 **Gene expression dynamics in developing Glass-3D^{+BMP} hPSC-amnion**
311 To identify key players potentially involved in amnion fate specification at different
312 stages, we comprehensively characterized all significantly upregulated genes based on
313 when significant upregulations are seen: "immediate" (**Table 2A**, up in 0.5- or 1-hr
314 samples), "early" (**Table 2B**, 3- or 6-hr), "intermediate-1" (**Table 2C**, 12-hr),
315 "intermediate-2" (**Table 2D**, 24-hr) and "late" (**Table 2E**, 48-hr); genes that were kept
316 after a more stringent filtering (described in Materials and Methods) are shown in **Fig.**
317 **6**), enabling the identification of additional temporal markers.
318 Previous studies have identified several *pan*-amnion markers that are known
319 immediate BMP targets (e.g., *GATA3* and others in the list of "immediate" genes, **Table**
320 **2A**), which are expressed in other early BMP-driven tissue morphogenesis. Among the
321 known *pan*-amnion markers, ISL1 is a highly promising marker for early lineage
322 specified amnion cells (Yang et al., 2021; Zhao et al., 2021; Zheng et al., 2022). In
323 accord with this, we found that ISL1 expression is limited to squamous amnion cells and
324 is not seen in the epiblast or in transitioning boundary cells (**Fig. 5B**). Notably, in Glass-
325 3D^{+BMP}, *ISL1* first shows a significant upregulation at 24-hr (intermediate -2, **Fig. 7A**).
326 This correlates with the timeframe at which squamous cells are first observed (**Fig. 2**).
327 This finding suggests that amnion specification is likely initiated prior to 24 hours in
328 Glass-3D^{+BMP} and that genes that are upregulated between 12-24-hr could be used as
329 additional markers for amnion specification. Consistent with the studies by Tyser *et al.*,

330 we identified *DLX5* (716.76-fold increase between 12- and 24-hr, and 2.4-fold increase
331 from 24- to 48-hr, **Fig. 7B**). Interestingly, however, our expression analysis of the Tyser
332 *et al.* dataset reveals a broader *DLX5* expression pattern compared to *ISL1* (the ISL1
333 expression domain map is similar to that of TFAP2A, **Fig. 4B**). Indeed, our IF analyses
334 for DLX5 in developing hPSC-amnion as well as in a CS7 cynomolgus macaque
335 embryo show expression patterns similar to TFAP2A (**Fig. 7C,D**). These results further
336 validate ISL1 as a marker for specified amnion cells and establish that DLX5 as an
337 additional marker for cells undergoing amniogenesis as well as mature amnion cells.
338

339 **Functional tests of an immediate-, GATA3, and an early-, TFAP2A, responding**
340 **transcription factors**

341 Immediate- and early-responding transcription factors are functionally relevant
342 candidates that initiate amnion specification and drive the expression of early amnion
343 lineage specified markers such as ISL1. Among the genes in the immediate- and early-
344 responding categories, we screened for genes associated with transcription, and
345 identified several genes, including immediate – GATA3 and early – TFAP2A. As noted
346 above, GATA3 expression precedes TFAP2A expression by approximately 12 hours.
347 Both of these factors show highly enriched expression, and both have previously
348 established functions as pioneer transcription factors (Rothstein and Simoes-Costa,
349 2020; Takaku et al., 2016; Tanaka et al., 2020; Van Otterloo et al., 2022; Zaret and
350 Carroll, 2011). Therefore, we examined the role of GATA3 and TFAP2A by generating
351 hPSC-amnion in Glass-3D^{+BMP} derived from H9 cells lacking GATA3 or TFAP2A (two
352 clonal lines with unique mutations were used for each analysis, see **Fig. S4** for KO

353 validation). Interestingly, *GATA3*-KO hPSC grown in Glass-3D^{+BMP} develop into fully
354 squamous cysts that express amnion markers, possibly indicating a functional
355 redundancy with other expressed GATA genes (e.g., GATA2, data not shown). In
356 contrast, while controls show uniformly squamous amniotic cells at 48-hr, *TFAP2A*-KO
357 cysts contain both squamous (ISL1^{+}) and columnar (NANOG^{+}/SOX2^{+}) cell populations
358 (**Fig. 8A** (Glass-3D hPSC-pluripotent cysts),**8B,C** (Glass-3D^{+BMP} hPSC-amnion cysts)):
359 these KO cysts display some resemblance to control 24-hr intermediate cysts (**Fig.
360 2B,C**). These results suggest that amniogenesis may be halted in the absence of
361 *TFAP2A*. To examine this further at transcriptomic levels, we performed time-course
362 bulk RNA-seq for control and *TFAP2A*-KO hPSC-amnion at 0-, 12-, 24- and 48-hr, and
363 performed a transcriptome similarity analysis using the Tyser et al. human CS7 embryo
364 dataset. Indeed, while an expected Epiblast to Ectoderm differentiation trajectory similar
365 to **Fig. 4C** is found in controls (**Fig. 8D**, left), *TFAP2A*-KO samples do not overlap with
366 Ectoderm cells, even at 48-hr (**Fig. 8D**, right). Rather, 48-hr *TFAP2A*-KO samples show
367 transcriptomic characteristics similar to some Primitive Streak cells (**Fig. 8D**, uncropped
368 plots shown in **Fig. S5**). These results reveal a paused amniogenesis phenotype in the
369 absence of TFAP2A, providing a previously unrecognized notion that TFAP2A is critical
370 for maintaining amnion fate progression.
371

372 **DISCUSSION**

373 In this study, we developed a reproducible and faithful model for robust mechanistic
374 examinations of human amnion fate specification, and identified a BMP4-dependent
375 amniogenic transcriptional cascade, as well as a role for TFAP2A in maintaining amnion

376 fate progression. Moreover, we established DLX5 as an additional marker for lineage
377 progressing amnion cells, and provided evidence for an active amniogenic
378 transcriptional cascade at the epiblast/amnion boundary in peri-gastrula human and
379 non-human primate embryos. These findings and the temporally resolved amniogenic
380 gene lists provided in this study offer additional avenues for further exploration of
381 human amniogenesis.

382 Previous studies established several broad amnion markers (e.g., GATA3,
383 TFAP2A and ISL1) that are expressed in developing, as well as, differentiated amnion
384 cells. However, comprehensive studies have not been performed to fully characterize
385 how each of these markers corresponds to amnion fate specification steps, especially
386 since BMP signaling is a primary trigger of amniogenesis and a large set of BMP target
387 genes are activated. In this study, a time-course transcriptomic analysis was employed
388 to identify genes that display temporal-specific dynamics among genes that show more
389 static expression patterns: this enabled us to define “stage specific” genes that can be
390 used to distinguish amniogenic fate progression states. In particular, we found that
391 *GATA3* is an immediate BMP target during amniogenesis (along with other known
392 targets such as *ID1*, *ID2* and *BAMBI*); a similar BMP4 → GATA3 transcriptional pathway
393 has been well-established previously in other systems (Abe et al., 2021; Bonilla-Claudio
394 et al., 2012; Gunne-Braden et al., 2020; Vincentz et al., 2016).

395 Early activation of GATA3 is followed by the expression of second-tier “early”
396 genes such as *TFAP2A* by 6-hr (clear TFAP2A protein is detected by 12-hr). Our
397 functional analyses indicate that loss of TFAP2A results in incomplete amniogenesis,
398 with failure to downregulate pluripotent genes and loss of some differentiated amnion

399 markers. Thus, TFAP2A, a previously recognized pioneer factor (Rothstein and Simoes-
400 Costa, 2020; Van Otterloo et al., 2022), appears to be an important component that
401 ensures the proper progression of the amniogenesis process.

402 Several hours following the activation of *TFAP2A*, third-tier "intermediate" genes
403 such as *ISL1* (ISL1 protein by 24-hr: only in squamous cells) are expressed. It has been
404 previously established that *ISL1* is a key amnion marker in early primate embryos (Yang
405 et al., 2021; Zhao et al., 2021; Zheng et al., 2022). Interestingly, our IF analyses of early
406 peri-gastrulation cynomolgus macaque embryos show that ISL1 expression is restricted
407 to amnion cells that are already squamous in nature (**Fig. 5**). Additionally, our time-
408 course transcriptomic analyses in Glass-3D^{+BMP} reveal that *ISL1* expression is seen at
409 12-24-hr, later than *TFAP2A* activation but much earlier than activation of more
410 differentiated amnion markers such as *GABRP*, *EPAS1* and *IGFBP3* (48-hr). Together,
411 these results suggest that amnion cells progress from GATA3^{+}, to GATA3^{+}/TFAP2A^{+}, to
412 GATA3^{+}/TFAP2A^{+}/ISL1^{+}, to mature amnion cells that express these three markers as
413 well as the more mature amnion markers such as GABRP, EPAS1 and IGFBP3.

414 The first amniogenesis event is seen upon implantation, in the epiblast cells
415 underlying the polar trophectoderm, establishing the amniotic sac, an asymmetric
416 amnion-epiblast cystic structure (Enders et al., 1983; Enders et al., 1986; Shahbazi and
417 Zernicka-Goetz, 2018; Taniguchi et al., 2017). In this study, we provide evidence for the
418 active progression of amniogenic fate conversion at the amnion-epiblast boundary of
419 the cynomolgus macaque peri-gastrula. What is the difference between amniogenesis
420 that occurs during implantation and during gastrulation? A previous study by Sasaki *et*
421 *al.* (Sasaki et al., 2016) showed that, in a macaque embryo staged at PreG1 (just

422 initiating implantation), a stage before *BMP4* expression is seen in the amnion at
423 PreG2, *BMP2* is abundantly expressed in the visceral endoderm. However, the visceral
424 endoderm underlies the epiblast population that gives rise to the embryo proper (not
425 amnion), and *CER1* is also abundantly expressed in the visceral endoderm (Sasaki et
426 al., 2016). Thus, BMP2 in the visceral endoderm in PreG1 embryo is thought not to be
427 the trigger for the initial amniogenesis processes that forms the amniotic sac, and it is
428 currently unclear how BMP signaling is activated in the nascent amnion cells during
429 implantation *in vivo*. Using a Gel-3D hPSC-amnion system, we previously showed that
430 amniogenesis is mechanosensitive, and that a soft substrate can induce BMP signaling
431 in a mechanically dependent manner in developing hPSC aggregates/cysts. This
432 suggests that mechanical signaling might play an important role in the initial BMP
433 signaling activation and downstream amniogenesis during implantation *in vivo*. In
434 contrast, since a continuous BMP signaling cascade is established in epiblast cells of
435 the early primate gastrula (e.g., driving primitive streak formation, primordial germ cell
436 formation), we speculate that the amniogenesis process that occurs during and post
437 gastrulation may be independent of a mechanical cue. It is, however, important to note
438 that the pluripotency states are distinct in the epiblast cells during implantation
439 compared to during gastrulation; it has been suggested that the epiblast cells are in the
440 formative state during implantation and in the primed state during gastrulation (Kinoshita
441 and Smith, 2018; Shahbazi et al., 2017; Smith, 2017). Thus, it is possible that the
442 mechanisms regulating responses to BMP ligands, as well as BMP-dependent
443 transcriptional machineries may differ.

444 Overall, our detailed temporally resolved analyses of Glass-3D^{+BMP} hPSC-
445 amnion development, combined with validation in early macaque embryos has revealed
446 several previously unrecognized findings with implications for BMP-dependent
447 amniogenic transcriptional machineries during amniogenesis, mechanisms continuing
448 amniogenesis in peri-gastrula macaque embryos, and functional characterization of the
449 transcriptional machinery required for amnion fate specification.
450

451 **MATERIALS AND METHODS**

452 *hESC lines*

453 Human embryonic stem cell line H9 was used in this study (WA09, P30, P48, WiCell;
454 NIH registration number: 0062). All protocols for the use of hPSC lines were approved
455 by the Human Stem Cell Research Oversight Committee at the Medical College of
456 Wisconsin. All hPSC lines were maintained in a feeder-free system for at least 20
457 passages and authenticated as karyotypically normal at the indicated passage number.
458 Karyotype analysis was performed at Cell Line Genetics. All hPSC lines tested negative
459 for mycoplasma contamination (LookOut Mycoplasma PCR Detection Kit, Sigma-
460 Aldrich). All transgenic and KO hESC lines in this study used H9 as the parental line. In
461 summary, hESC were maintained in a feeder-free culture system with mTeSR1
462 medium, or with 50%/50% mix of mTeSR1 and mTeSR plus (STEMCELL
463 Technologies). hESC were cultured on 1% (v/v) Geltrex (Thermo Fisher Scientific), or
464 with Cultrex SCQ (Bio-techne) coated 6 well plates (Nunc). Cells were passaged as
465 small clumps every 4 to 5 days with Dispase (Gibco). All cells were cultured at 37°C
466 with 5% CO_2. Media was changed every day. hESC were visually checked every day to

467 ensure the absence of spontaneously differentiated, mesenchymal-like cells in the
468 culture. Minor differentiated cells were scratched off the plate under a dissecting scope
469 once identified. The quality of all hESC lines was periodically examined by
470 immunostaining for pluripotency markers and successful differentiation to three germ
471 layer cells.
472
473 *Cynomolgus macaque*
474 *Animals*
475 The female and male cynomolgus macaque were housed and cared for at the Wisconsin
476 National Primate Research Center (WNPRC). All procedures were performed in
477 accordance with the NIH Guide for the Care and Use of Laboratory Animals and under
478 approval of the University of Wisconsin College of Letters and Sciences and Vice
479 Chancellor Office for Research and Graduate Education Institutional Animal Care and
480 Use Committee (protocol g005061).
481
482 *Animal breeding and pregnancy detection*
483 Beginning on day 8 post-onset of menses, the female was housed with a compatible
484 male and monitored for breeding. Animals were pair-housed until day 16-20 post-onset
485 of menses. A 2-3 mL blood draw was performed daily from day 8 post-onset of menses
486 until day 16 to assess the timing of ovulation based on the estradiol peak and rise in
487 progesterone in serum. Serum samples were analyzed for estradiol (25 μL) and
488 progesterone (20 μL) using a cobas e411 analyzer equipped with
489 ElectroChemiLuminescence technology (Roche, Basal, Switzerland) according to

490 manufacturer instructions. Results were determined via a calibration curve which was
491 instrument-generated by 2-point calibration using traceable standards and a master
492 curve provided via the reagent barcode. Inter-assay coefficient of variation (CV) was
493 determined by assaying aliquots of a pool of rhesus plasma. For estradiol, the limit of
494 quantitation (LOQ) was 25 pg/mL, the intra-assay CV was 2.02%, and the inter-assay
495 CV was 5.05%. For progesterone, the LOQ was 0.2 ng/mL, the intra-assay CV was
496 1.37%, and the inter-assay CV was 4.63%. A transabdominal ultrasound was performed
497 to detect pregnancy as early as 14 days post-ovulation. The ultrasound measurements
498 in combination with the timing of ovulation were used to estimate the day of conception
499 and gestational age of the pregnancy.
500
501 *Terminal perfusion uterine collection, paraffin embedding, sectioning and staining*
502 The pregnant female was sedated with intramuscular ketamine (>15 mg/kg) followed by
503 IV sodium pentobarbital (>35 mg/kg) and then perfused with 4% paraformaldehyde (PFA)
504 via the left ventricle. The entire uterus and cervix were removed. The serosa and
505 superficial myometrium were scored for better fixative penetration and to denote dorsal
506 and ventral orientation. Tissues were fixed in 4% PFA with constant stirring and solution
507 changes were performed every 24 hours for a total of 72 h. The uterus was serially
508 sectioned from the fundus to the internal cervical os into 4 mm slices using a dissection
509 box. Cassettes with tissue sections were transferred into 70% ethanol, routinely
510 processed in an automated tissue processor and embedded in paraffin for histological
511 analyses (5 μm sections). Fixed uterine tissue were cut in 5 μm thick cross-sections,
512 mounted on slides, deparaffinized in xylene and rehydrated in an ethanol series. Antigen

513 retrieval was performed by boiling in citrate buffer. Sections were blocked 4% goat serum
514 in PBS at RT for at least 3-hr. Subsequent immunolocalization was performed using
515 commercially available primary antibodies, incubated overnight at 4 °C in 4% serum, at
516 the dilutions as shown in **Table 3**. Immunofluorescent detection was performed using
517 secondary antibodies tagged with a fluorescent dye (fluorophores excitation = 488, 555,
518 and 647nm), and counterstained with DAPI. Negative controls were performed in which
519 the primary antibody was substituted with the same concentration of normal IgG of the
520 appropriate isotype. Images were obtained with a Zeiss LSM980 microscope.
521
522 *Glass-3D^{+BMP} hPSC-amnion formation assays*
523 Glass-3D protocol used to generate hPSC-pluripotent cysts was previously described
524 (Hamed et al., 2023; Shao et al., 2017a; Taniguchi et al., 2017; Taniguchi et al., 2015).
525 In brief, hPSC monolayers were dissociated using Accutase (Sigma-Aldrich) at 37 °C for
526 10 min, centrifuged and resuspended in mTeSR1/mTeSR plus 50:50 mix containing 10
527 μM Y-27632 (STEMCELL Technologies). hPSC were plated as single cells at 20,000
528 cells cm^{-2}, unless otherwise specified, onto a 1% (v/v) gel coated wells (Geltrex
529 (Thermo Fisher Scientific), or with Cultrex SCQ (Bio-techne)). After 24 hours (on day 1),
530 culture medium was replenished with fresh mTeSR1/mTeSR plus 50:50 media without
531 Y-27632, supplemented with 2% (v/v) Geltrex or with Cultrex SCQ. Thereafter, media
532 change was performed daily until day 4 (using mTeSR1/mTeSR plus 50:50 media
533 supplemented with 1% (v/v) Geltrex or with Cultrex SCQ), unless otherwise noted. This
534 Glass-3D culture condition results in the formation of hPSC-cysts, cysts with a central
535 lumen surrounded by pluripotent columnar cells. The Glass-3D^{+BMP} culture condition

536 was used to generate hPSC-amnion, cysts with a central lumen surrounded by
537 squamous amnion-like cells. To induce amniogenesis, exogenous BMP ligand
538 (20ng/mL, Bio-techne) was added to developing pluripotent cysts between day 2 to 3 for
539 24 hours, or between day 2 to 4 for 48 hours, unless otherwise noted (e.g., for time-
540 course analyses). Samples were harvested at day 4 (48-hr since starting BMP4
541 treatment). LDN-193189 (500nM, STEMCELL Technologies) was used to disrupt BMP
542 signaling.
543
544 *DNA constructs*
545 *piggyBac-CRISPR/Cas9 (pBACON) constructs*
546 A piggyBac-CRISPR/Cas9 (pBACON) vector that contains SpCas9-T2A-puro and hU6-
547 gRNA expression cassettes flanked by piggyBac transposon terminal repeat elements
548 (pBACON-puro), which allows subcloning of annealed oligos containing gRNA
549 sequence at *BbsI* site, has been previously described (Shao et al., 2017b; Townshend
550 et al., 2020; Wang et al., 2021). gRNA targeting genomic sites and oligo sequences to
551 generate pBACON-GFP-h*GATA3* (primers: CRISPR_hGATA3_CDS1#1_s and
552 CRISPR_hGATA3_CDS1#1_as) and -h*TFAP2A* (CRISPR_hTFAP2A_CDS2_s and
553 CRISPR_hTFAP2A_CDS1_as) are found in **Fig. S4** and **Table 3B**; these were
554 designed using publicly available tools (http://crispr.mit.edu or
555 https://www.idtdna.com/site/order/designtool/index/CRISPR_CUSTOM).
556
557 *piggyBac-based transgenic and genome edited hESC lines*

558 PB constructs (3μg) and pCAG-ePBase (Lacoste et al., 2009) (1μg) were co-transfected
559 into H9 hESC (70,000 cells cm^{-2}) using GeneJammer transfection reagent (Agilent
560 Technologies). To enrich for successfully transfected cells, drug selection (puromycin,
561 2μg/mL for 4 days; neomycin, 250μg/mL for 5 days) was performed 48 to 72 hours after
562 transfection. hESC stably expressing each construct maintained the expression of
563 pluripotency markers. For inducible constructs, DOX (500ng/mL) treatment was
564 performed for 48 hours for neomycin-selected *TFAP2A*-KO rescue pools.
565 During pBACON-based genome editing, puro-selected cells were cultured at low
566 density (300 cells cm^{-2}) for clonal selection. Established colonies were manually picked
567 and expanded for screening indel mutations using PCR amplification of a region
568 spanning the targeted gRNA region (genomic DNA isolated using DirectPCR Lysis
569 Reagent (Tail) (VIAGEN), primers: hGATA3, PCR_GATA3_RI_fw#2 and
570 PCR_GATA3_NI_rv#2; hTFAP2A, PCR_TFAP2A_RI_fw and PCR_TFAP2A_NI_rv),
571 which were subcloned into pPBCAG-GFP (Chen and LoTurco, 2012) at EcoRI and NotI
572 sites, and sequenced (Seq-3'TR-pPB-Fw). At least 12 to 15 bacterial colonies were
573 sequenced to confirm genotypic clonality. Western blots for each protein were also
574 performed to further validate the KO lines. Control cells are H9 hESC in all loss-of-
575 function experiments.
576
577 *Western blot*
578 SDS PAGE gels (10%) and PVDF membranes were used. Membranes were blocked
579 using Intercept (TBS) Blocking Buffer (Licor), total protein quantification was performed
580 by using Revert 700 Total Protein Stain (Licor), and primary antibody overnight

581 incubation was performed at 4˚C, followed by 30-min IRDye (Licor) secondary antibody
582 incubation at room temperature. Blots were imaged using Licor Odyssey Infared
583 Imaging system.
584
585 *Immunostaining*
586 hPSC staining protocols have been previously described (e.g., (Hamed et al., 2023;
587 Shao et al., 2017a; Wang et al., 2021)). In short, samples (hPSC-cysts, hPSC-amnion)
588 grown on the coverslip were rinsed with phosphate-buffered saline (PBS; Gibco) twice,
589 fixed with 4% paraformaldehyde (Sigma-Aldrich) in 1x PBS for 40 to 60 min, then rinsed
590 with PBS three times, and permeabilized with 0.1% SDS (Sigma-Aldrich) solution for 40
591 min. The samples were blocked in 4% heat-inactivated goat serum (Gibco) or 4%
592 normal donkey serum (Gibco) in PBS 1 hour to overnight at 4°C. The samples were
593 incubated with primary antibody solution prepared in blocking solution at 4°C overnight,
594 washed three times with PBS (10 min each), and incubated in blocking solution with
595 goat or donkey raised Alexa Fluor–conjugated
596 secondary antibodies (Thermo Fisher Scientific) at room temperature for 2 hours. DNA
597 counterstaining was performed using Hoechst 33342 (nucleus, Thermo Fisher
598 Scientific), Alexa Fluor–conjugated WGA (membrane, Thermo Fisher Scientific). All
599 samples were mounted on slides using 90% glycerol (in 1x PBS). When mounting cyst
600 samples, modeling clays were used as spacers between coverslips and slides to
601 preserve lumenal cyst morphology.
602
603 *Confocal microscopy, live imaging and image analysis*

604 Confocal Images of fixed samples were acquired using Zeiss LSM980 microscope.
605 Measurements of cell nucleus dimensions, cyst epithelial thickness, and cyst orientation
606 angle were performed manually using the Measurement tool in ImageJ (NIH).
607
608 *RNA isolation and qRT-PCR analysis*
609 Total RNA extraction was performed using TRIzol (Thermo Fisher). The quantity and
610 quality of total RNA was determined by spectrometry and denaturing agarose gel
611 electrophoresis, respectively. The cDNA was synthesized from total RNA (1μg) using
612 High-Capacity cDNA Reverse Transcription Kit (Applied Biosystems). Quantitative real-
613 time RT-PCR (qPCR) analysis of mRNA expression was performed using a CFX96
614 Real-Time PCR Detection System (BioRad) with Power Up™ SYBR Green Master Mix
615 (Applied Biosystems). Primers (**Table 3B**) were designed using NCBI primer design tool
616 to span at least one exon/intron junction. Data were normalized against *GAPDH* and are
617 shown as the average fold increase ± standard error of the mean (SEM) with relative
618 expression being calculated using the 2-ΔΔCT method as described previously (Livak
619 and Schmittgen, 2001). After amplification, the specificity of the PCR was determined by
620 both melt-curve analysis and gel electrophoresis to verify that only a single product of
621 the correct size was present.
622
623 *RNA sequencing and bioinformatics*
624 The quality of total RNA was determined using TapeStation RNA ScreenTape. RNA
625 was enriched for mRNA using NEBNext Poly(A) mRNA Magnetic Isolation Module
626 (E7490). cDNA and library preparation were performed using NEBNext® Ultra™ II

627 Directional RNA Library Prep kit for Illumina (New England Biolabs). Library
628 concentration was determined using NEBNext® Library Quant Kit for Illumina (New
629 England Biolabs) or by Qubit (Thermo). Samples were then pooled and were
630 sequenced using Illumina sequencers: NextSeq550 (Versiti Blood Research Institute) or
631 using NovaSeq 6000 (S4 flowcell, the DNA services laboratory of the Roy J. Carver
632 Biotechnology Center at the University of Illinois at Urbana-Champaign). Sequence data
633 was analyzed using the RNA-Seq workflow in Partek Flow software (Partek Inc., St.
634 Louis, MO, USA). Raw sequencing reads were mapped to the human genome hg38
635 using STAR version 2.7.8a with default parameter settings. Aligned reads were then
636 quantified to Ensembl Transcripts release 104 using Partek's method and genes with
637 fewer than 10 reads in all samples were excluded from the subsequent analyses. Gene
638 counts were then filtered based on gene_biotype for protein_coding genes, followed by
639 excluding features where maximum <= 30.0 reads. Gene expression was then
640 normalized using DESeq2 (Median Ratio). Differentially expressed genes were selected
641 using as criteria FDR < 0.05 and absolute fold change > 2.
642
643 *GO enrichment analysis*
644 GO analysis were performed on significantly upregulated (1,820) or downregulated
645 (2,092) genes in Glass-3D^{+BMP} amnion-cysts vs Glass-3D pluripotent-cysts (From **Fig.**
646 **3**).
647
648 *Mapping and gene expression analyses of Tyser et al. Carnegie Stage 7 human embryo*
649 *single cell RNA sequencing dataset*

650 The original UMAP coordinates and annotations for all 1,195 cells were used
651 throughout. The processed data were downloaded from http://www.human-gastrula.net,
652 which was used to generate a UMAP plot (using DimPlot in R package Seurat), as well
653 as to perform expression analyses (FeaturePlot in Seurat).
654
655 *RNA velocity (scvelo) analysis of Tyser et al. Carnegie Stage 7 human embryo single*
656 *cell RNA sequencing dataset*
657 RNA velocities across all 1,195 single cells were embedded on the original UMAP
658 coordinates shown in Tyser *et al.* (Tyser et al., 2021). The Tyser et al. Carnegie Stage 7
659 human embryo raw fastq dataset was obtained from ArrayExpress (accession code: E-
660 MTAB-9388). From the aligned BAM files, a loom file was generated using the function
661 run_smartseq2 mode in software velocyto (v0.17) with default parameters to create a
662 count matrix made of spliced and unspliced read counts (with Human genome
663 annotation hg19). scVelo (Python package v.0.2.5 (Bergen et al., 2020) was used to
664 examine inferred RNA velocity and visualized the velocities on the UMAP embedding by
665 stream plot (with default parameters except smooth was set to 1).
666
667 *Transcriptomic similarity analysis between bulk RNA sequencing and Tyser et al.*
668 *Carnegie Stage 7 human embryo single cell RNA sequencing datasets*
669 Transcriptomic similarities between bulk RNA sequencing samples and the Tyser *et al.*
670 dataset were examined and visualized using original UMAP coordinates from Tyser *et*
671 *al.*. In summary, each bulk RNA-seq sample was first downsampled to 100 pseudo-
672 single cell data using R package projectLSI (Granja et al., 2019), which was followed by

673 data integration with Tyser *et al.* dataset in UMAP dimension reduction space. A medoid
674 from 100 pseudo-single cell data was used as the representation of each bulk RNA-seq
675 sample, and, for each sample, we identified the most transcriptomically similar cell from
676 Tyser *et al.* dataset, based on Euclidean distance on UMAP space.
677
678 *Data availability*
679 The raw data, unfiltered count matrix and processed count matrix will be available to the
680 database of Genotypes and Phenotypes (dbGaP) upon publication.
681
682 *Statistical analyses*
683 Graphs were generated using Prism 7 (GraphPad Software) or R,
684 and statistical analyses were performed using Prism 7. Fig. 1D, 5 independent samples
685 were counted at each timepoint (total of > 50 cells/sample). For analysis we used one-
686 way ANOVA with post-hoc Dunnet's multiple comparisons test. In Fig. 1K, 3
687 independent samples were counted (total of > 75 cells were plotted). For analysis we
688 used two-tail Student-T test. In Fig. 1J, 3 independent samples were counted (total of >
689 50 cells were plotted). For analysis we used one-way ANOVA with post-hoc Tukey's
690 multiple comparison test. In Fig. 2, relative mRNA expression was detected in n=3 for
691 each timepoint. For analysis we used one-way ANOVA with post-hoc Tukey's multiple
692 comparison test. *, significant (p-value<0.05); ns, non-significant. All experiments were
693 repeated at least three times.
694
695 **FIGURE LEGENDS**

696 **Figure 1. Highly penetrant amniogenesis in a Glass-3D^{+BMP} culture system.** (**A**,**B**)
697 hPSC-derived pluripotent cyst (hPSC-pluripotent cyst, Glass-3D in (**A**)) and amnion cyst
698 (Glass-3D^{+BMP} in (**B**)) assays. BMP4 treatment (20ng/mL) leads to uniformly squamous
699 amnion cysts by Day 4. (**C**) Confocal optical sections of d2 cysts harvested prior to (0-
700 min) and 10-, 20-, 30- and 60-min after BMP4 treatment, stained with indicated markers.
701 Staining for phosphorylated SMAD1/5 reveals a prominent nuclear pSMAD1/5
702 enrichment within 10-min of BMP4 treatment in all cells. (**D**) Quantification of nuclear
703 pSMAD1/5: five independent samples were counted, more than 50 cells were counted
704 per sample. * indicates statistically significant changes ($p<0.05$) compared to 0-min
705 timepoint. (**E**) Abundant GATA3 expression (in green), but not TFAP2A (red), is seen by
706 3 hours after BMP4 treatment while SOX2 expression is maintained. (**F-H**) Pluripotency
707 (NANOG, SOX2) and amnion (ISL1/2, GATA3, TFAP2A) marker expression analyses of
708 d4 cysts grown in the Glass-3D (top) or in Glass-3D^{+BMP} (bottom) conditions. (**I,J**)
709 Confocal micrographs of d4 cysts grown in the Glass-3D^{+BMP} system stained for
710 phosphorylated EZRIN, RADIXIN and MOESIN (pERM), an apical membrane marker,
711 as well as with indicated amnion markers (top – cysts were treated with BMP4 for 24
712 hours between d2 and d3; bottom – treated with BMP4 for 48 hours from d2 to d4).
713 (**K,L**) Quantification of GATA3 and ISL1/2 fluorescent intensities in 24- (blue, n = 115
714 cells) and 48-hr (red, n = 76 cells) BMP4 treatment samples (**K**), as well as of nuclear
715 aspect ratios of d4 hPSC-cyst (black, n = 63 cells), and 24- (blue, n = 45 cells) and 48-
716 hr (red, n = 52) BMP4-treated cysts (harvested at d4), (**L**). (**M**) pSMAD1/5 staining
717 (green) shows similar nuclear enrichment between 24- and 48-hr BMP4 treatment at d4
718 (also stained with indicated markers). Scale bars = 50μm.

719

720 **Figure 2. Time-course analysis of Glass-3D^{+BMP} hPSC-amnion development.** (**A**)
721 Timeline of the Glass-3D^{+BMP} hPSC-amnion assay. Twenty four-hr BMP treatment is
722 sufficient to generate uniformly squamous hPSC-amnion cysts. (**B,C**) Optical sections of
723 time-course Glass-3D^{+BMP4} hPSC-amnion cysts (harvested at indicated timepoints after
724 BMP4 treatment) stained with indicated markers (inverted black and white fluorescent
725 signals shown for individual channels, to aid visualization). GATA3, an immediate BMP
726 target is seen by 3-hr (yellow arrowheads). hPSC-amnion cysts with prominent nuclear
727 TFAP2A (**B**) and ISL1/2 (**C**) are seen by 12- and 24-hr, respectively (yellow
728 arrowheads), while SOX2 shows gradual decrease. Consistent changes are also
729 observed at mRNA transcript levels using quantitative RT-PCR (**D-F**, also see the
730 expression of additional markers: *HAND1* (amniotic) and *NANOG* (pluripotent); *
731 indicates statistically significant changes ($p<0.05$) compared to 0-hr timepoint). (**G**)
732 Relative mRNA expression analyses of indicated pluripotency (top) and amniotic
733 (bottom) markers between d4 Glass-3D hPSC-pluripotent cyst (black), and d4 Glass-
734 3D^{+BMP} hPSC-amnion with 24-hr (blue) or 48-hr (red) BMP treatment; * indicates
735 statistically significant changes ($p<0.05$). (**H**) BMP inhibitor (LDN-193189) treatment
736 outline as well as confocal micrographs of d4 Glass-3D^{+BMP} hPSC-amnion (top, control
737 – 24-hr BMP4 treatment between d2 and d3) and hPSC-amnion treated with LDN-
738 193189 between d3 and d4 after BMP4 treatment (between d2-d3). Scale bars = 50μm.

739

740 **Figure 3. Temporally-resolved transcriptomic characterization of Glass-3D^{+BMP}**
741 **hPSC-amnion.** (**A**) Experimental timeline (from d2) of the time-course bulk RNA

742 sequencing analysis. Colored arrowheads indicate timepoints at which samples were
743 harvested. (**B**) A heatmap showing a hierarchical clustering analysis of all detected
744 genes (12,940): bulk transcriptomes from triplicate samples are shown at each
745 timepoint. A gradient scale indicates Z-score. (**C**) Principal component analysis (PCA)
746 plot of time-course bulk transcriptomes, using the most variable genes, revealing
747 progressive transcriptomic changes overtime (indicated by the dotted arrow). Note that
748 coloring is consistent with the arrowheads in (**A**). (**D**-**G**) Time-course plots of normalized
749 expression values for selected known immediate BMP target (**D**), general amnion (**E**),
750 advanced amnion (**F**) and pluripotency genes (**G**). (**H**) A volcano plot analysis showing
751 up- (red) and down- (blue) regulated genes in Glass-3D^{+BMP} hPSC-amnion cysts (gene
752 expression compared to d4 pluripotent hPSC-cysts): black lines represent cutoffs for p-
753 value <0.05 and 2-fold difference.
754
755 **Figure 4. Transcriptome comparison of developing Glass-3D^{+BMP} hPSC-amnion**
756 **cysts and a Carnegie stage (CS) 7 human embryo.** (**A**) A UMAP plot displaying the
757 original single cell transcriptome coordinates of the CS7 human embryo described in
758 Tyser *et al.*, shown with the original annotations. The inset (**i**) is used for expression
759 analyses in (**B**). (**B**) Expression of amnion markers – *GATA3*, *TFAP2A* and *ISL1* –
760 superimposed onto the UMAP plot in (**A** – **i**). (**C**) Transcriptome similarity analysis
761 comparing the CS7 human embryo single cell dataset and the Glass-3D^{+BMP} time-
762 course bulk RNA-seq dataset, showing the human CS7 embryo UMAP plot (inset) with
763 colored cells that are transcriptomically similar to each timepoints as indicated (orange –
764 pluripotent cysts/monolayer and 0-, 0.5-, 1-, 3- and 6-hr post-BMP4; green – 12-hr post-

765 BMP4; blue – 24-hr; magenta – 48-hr). While pluripotent and earlier timepoints (orange
766 colored cells) overlaps with Epiblast cells, some 12-hr (green) and all 24-hr (blue)
767 samples are similar to a subpopulation of Primitive Streak cells, and 48-hr (magenta)
768 samples overlap exclusively with Ectoderm (see Materials and Methods for detailed
769 bioinformatics pipeline). (**D**) *TBXT* expression transposed onto the CS7 human embryo
770 UMAP plot, revealing *TBXT*^{low} Primitive Streak sub-population that show transcriptomic
771 similarities to 24-hr post-BMP samples (indicated by dotted circle). Gradient scales
772 indicate expression level (orange = high, gray = low). Uncropped plots are found in **Fig.**
773 **S2**.
774
775 **Figure 5. Transcriptional characterizations of amnion-epiblast squamocolumnar**
776 **boundary of the CS6/7 cynomolgus monkey amniotic sac.** (**A**) RNA velocity
777 analysis (scvelo) of the *Tyser et al.* CS7 human embryo dataset, showing predicted
778 lineage progression trajectories from Epiblast to Ectoderm traversing the *TBXT*^{low}
779 Primitive Streak sub-population. (**B-G**) Optical sections of a CS6/7 cynomolgus
780 macaque embryo stained for indicated transcription factors (GATA3, ISL1/2, pSMAD1/5
781 and SOX2 (**B**,**D**,**F**)), as well as quantitation for relative fluorescent intensity in proximal
782 (closer to epiblast) to distal (closer to amnion) cells of indicated markers at the amnion-
783 epiblast boundary (**C**, **E** and **G** are quantitation of images in **B**, **D** and **F**, respectively).
784 Each dot represents a single cell. (**i**), (**ii**) and (**iii**) indicate insets in (**F**). Half of the
785 amniotic sac shown. Quantitation shows that, while GATA3^{+}/TFAP2A^{+} cells are also
786 SOX2^{+}, ISL1^{+} cells are only seen after SOX2 expression is no longer detected: ISL1
787 expression is exclusive to squamous amnion cells. Moreover, the expression of

788 pSMAD1/5 and TFAP2A is reduced in most distal amnion (**ii**, **iii**). Scale bars 200μm. (**H**)
789 Nuclear aspect ratio quantitation of amnion-epiblast boundary cells in (**B**), (**C**) and (**D**),
790 mean+SEM shown. Dotted vertical line in each plot indicates amnion-epiblast boundary
791 (**C**,**E**,**G**,**H**). (**I**) A schematic representation of the CS6/7 cynomolgus macaque amniotic
792 sac: the confocal micrographs in (**B**) were edited to represent $SOX2^{+}$ epiblast
793 (pseudocolored in blue), primitive streak-derived disseminating (green),
794 $GATA3^{+}/TFAP2A^{+}/SOX2^{low}$ transition boundary (magenta) and $GATA3^{+}/TFAP2A^{+}/ISL1^{+}$
795 lineage specified amnion (red) cells.
796
797 **Figure 6. Characterization of differentially expressed genes identified through the**
798 **Glass-3D^{+BMP} hPSC-amnion time-course sequencing analysis.** (**A-E**) Combined and
799 selected genes are shown for each category (A – immediate; B – early; C –
800 intermediate-1; D – intermediate-2; E – late). Genes for each category are selected
801 based on significant upregulation (FDR<0.05, fold>2, based on Z-scores) by 1-
802 (immediate, n = 5), 3- (early, n = 9), 6- to 12- (intermediate-1, n = 30), 24- (intermediate-
803 2, n = 178) and 48-hr (late, n = 157) post-BMP4 treatment, compared to the previous
804 timepoint. Vertical lines indicate timepoints at which significant changes are seen.
805
806 **Figure 7. Establishment of DLX5 as a new marker of amniogenesis similar to**
807 **TFAP2A.** (**A,B**) Expression analyses for *ISL1* (**A**) and *DLX5* (**B**) in the time-course bulk
808 RNA sequencing (top) and in the single cell CS7 human embryo (bottom) datasets. (**C**)
809 Confocal optical sections of Glass-3D hPSC-pluripotent cysts (left) and Glass-3D^{+BMP4}
810 hPSC-amnion cysts (right, harvested at d4) stained with indicated markers. (**D**)

811 Histological section of a cynomolgus monkey amniotic sac at CS7 stained with indicated
812 markers (SOX2^{+} epiblast; TFAP2A^{+}/DLX5^{+}/SOX2^{-} amnion). Insets (**i** and **ii**) indicate the
813 amnion-epiblast boundaries. DLX5 and TFAP2A share a similar expression pattern at
814 the boundary. Similar to pSMAD1/5 and TFAP2A (shown in **Fig. 5F**), most distal amnion
815 cells show reduced DLX5 expression. Surface ectoderm bridging neural ectoderm and
816 amniotic ectoderm is not seen at this stage. Amniotic mesenchyme is observed
817 underlying the TFAP2A^{+}/DLX5^{+} amniotic epithelium at this stage. Scale bars = 500μm.
818
819 **Figure 8. Analyses of Glass-3D^{+BMP} hPSC-amnion in control and *TFAP2A*-KO**
820 **background.** (**A,B**) Optical sections of control and *TFAP2A*-KO cysts in Glass-3D (**A**,
821 pluripotent) as well as in Glass-3D^{+BMP} (**B**). While control-like pluripotent cysts are
822 formed in Glass-3D, several NANOG^{+} cells are still seen in Glass-3D^{+BMP} in the
823 absence of *TFAP2A*. (**C**) Confocal micrographs of d4 control and *TFAP2A*-KO Glass-
824 3D^{+BMP} hPSC-amnion cysts stained with indicated markers, showing a d3-like
825 intermediate morphology with ISL1^{+}/SOX2^{-} and ISL1^{-}/SOX2^{+} cells. (**D**) Transcriptome
826 similarity analysis comparing the CS7 human embryo single cell dataset with the time-
827 course (0-, 12-, 24- and 48-hr post-BMP) bulk dataset from control and *TFAP2A*-KO
828 Glass-3D^{+BMP} hPSC-amnion. Orange, green, blue and magenta colored cells are
829 transcriptomically similar to 0-, 12-, 24- and 48-hr post-BMP bulk RNA sequencing
830 samples, respectively. While a clear differentiation trajectory from Epiblast to Ectoderm
831 is seen in control (left), a halted amnion lineage progression is seen in the *TFAP2A*-KO
832 background. Scale bars = 50μm.
833

834 **Table 1. Glass-3D^{+BMP} hPSC-amnion time-course bulk RNA sequencing dataset.**
835 (**A**) normalized and filtered count matrix of the time-course bulk-RNA sequencing. (**B-C**)
836 Gene expression comparison analysis between 48-hr (d4) Glass-3D^{+BMP} hPSC-amnion
837 and d4 Glass-3D hPSC-cysts: lists of 1,813 up-regulated (**B**) and 2,088 down- (**C**)
838 regulated genes. (**D-E**) Gene Ontology analyses (Biological Processes) for top all
839 significantly up- (**D**) and down- (**E**) regulated genes.
840
841 **Table 2. Lists of immediate, early, intermediate and late genes.** An excel file
842 containing temporally resolved gene lists: (**A**) immediate (0.5- and 1-hr, 57 genes); (**B**)
843 early (3- and 6-hr, 135 genes); (**C**) intermediate-1 (12-hr, 81 genes); (**D**) intermediate-2
844 (24-hr, 642 genes); (**E**) late (48-hr, 909 genes). Genes that showed significant
845 upregulation compared to the previous timepoint (e.g., 0.5-hr compared to 0-hr, 3-hr
846 compared to 1-hr) were retained. Duplicated genes found in the list from earlier
847 timepoint lists are removed. For example, *GATA3* is significantly upregulated throughout
848 the time course, but is only included in the immediate category. Genes with averaged
849 normalized counts < 100 were excluded.
850
851 **Table 3. Lists of reagents used in this study.** (**A-C**) Lists of antibodies (**A**), primers
852 (**B**) and plasmids (**C**).
853
854 **SUPPLEMENTARY FIGURE LEGENDS**

855 **Figure S1. Glass-3D^{+BMP} hPSC-amnion formation using 1196a.** Confocal
856 micrographs of 1196a human induced pluripotent stem cell line grown in the Glass-
857 3D^{+BMP} condition, stained with indicated markers. Scale bars = 50μm.
858
859 **Figure S2. Original UMAP plots.** (**A**) UMAP expression plots of the Tyser *et al.* CS7
860 human embryo single cell RNA sequencing dataset used in this study (*GATA3*,
861 *TFAP2A*, *ISL1, TBXT* and *DLX5*) as well as (**B**) time-course transcriptome similarity
862 UMAP plot.
863
864 **Figure S3. Quantitation for relative fluorescent intensity in proximal and distal**
865 **cells of indicated markers at the amnion-epiblast boundary in a CS7 cynomolgus**
866 **macaque embryo.**
867
868 **Figure S4. Validation of *GATA3*- and *TFAP2A*-KO hPSC lines.** (**A,B**) Sequenced
869 genotyping results of *GATA3*-KO #1 and #2 lines (**A**), representative sequence traces
870 for each mutations are shown in (**B**). (**C-E**) Genotyping results of *TFAP2A*-KO #1 and
871 #2 lines (**C**), representative sequence traces for each mutation are shown in (**D**).
872 Western blot analysis for TFAP2A in control and *TFAP2A*-KO #1 and #2 lysates (**E**, β-
873 ACTIN is used as a loading control).
874
875 **Figure S5. Uncropped transcriptional similarity UMAP plots for control and**
876 ***TFAP2A*-KO shown in Fig. 8D.**
877

878 **ACKNOWLEDGEMENTS**

879 We thank A. Brivanlou (Rockefeller University) for ePB transposase. We thank Michaela
880 Patterson, Matthew Veldman and Deborah Gumucio for their insightful comments to the
881 manuscript, as well as Versiti Blood Research Institute Molecular Biology Core Lab and
882 the DNA Services laboratory of the Roy J. Carver Biotechnology Center at the
883 University of Illinois at Urbana-Champaign for sequence services. We also thank the
884 Wisconsin National Primate Research Center (WNPRC) Veterinary, Scientific Protocol
885 Implementation, Pathology and Animal Services Unit staff for providing animal care, and
886 assisting in procedures including breeding, pregnancy monitoring, and sample
887 collection. The contents of this manuscript are solely the responsibility of the authors
888 and do not represent the official views of the NIH.

889 **Funding:** This work was supported by NIH grants R01-HD098231 (K.T.) and P51-
890 OD011106 (to the WNPRC) as well as by MCW CBNA Start-up funds (K.T.).

891 **Competing interests:** The authors declare no competing interest. **Data and materials**
892 **availability**: All data needed to evaluate the conclusions in the paper are present in the
893 paper and the Supplementary Materials. Further information and requests for reagents
894 may be directed to Kenichiro Taniguchi.

895

896 **REFERENCES**

897 Abe, M., Cox, T.C., Firulli, A.B., Kanai, S.M., Dahlka, J., Lim, K.C., Engel, J.D., and
898 Clouthier, D.E. (2021). GATA3 is essential for separating patterning domains during
899 facial morphogenesis. Development *148*.

900 Beddington, R.S., and Robertson, E.J. (1999). Axis development and early asymmetry
901 in mammals. Cell *96*, 195-209.
902 Bergen, V., Lange, M., Peidli, S., Wolf, F.A., and Theis, F.J. (2020). Generalizing RNA
903 velocity to transient cell states through dynamical modeling. Nature biotechnology *38*,
904 1408-1414.
905 Bergmann, S., Penfold, C.A., Slatery, E., Siriwardena, D., Drummer, C., Clark, S.,
906 Strawbridge, S.E., Kishimoto, K., Vickers, A., Tewary, M.*, et al.* (2022). Spatial profiling
907 of early primate gastrulation in utero. Nature *609*, 136-143.
908 Bonilla-Claudio, M., Wang, J., Bai, Y., Klysik, E., Selever, J., and Martin, J.F. (2012).
909 Bmp signaling regulates a dose-dependent transcriptional program to control facial
910 skeletal development. Development *139*, 709-719.
911 Carleton, A.E., Duncan, M.C., and Taniguchi, K. (2022). Human epiblast
912 lumenogenesis: From a cell aggregate to a lumenal cyst. Seminars in cell &
913 developmental biology *131*, 117-123.
914 Chen, F., and LoTurco, J. (2012). A method for stable transgenesis of radial glia lineage
915 in rat neocortex by piggyBac mediated transposition. Journal of neuroscience methods
916 *207*, 172-180.
917 Chen, H.M., DeLong, C.J., Bame, M., Rajapakse, I., Herron, T.J., McInnis, M.G., and
918 O'Shea, K.S. (2014). Transcripts involved in calcium signaling and telencephalic
919 neuronal fate are altered in induced pluripotent stem cells from bipolar disorder patients.
920 Translational psychiatry *4*, e375.

921 Chen, K., Zheng, Y., Xue, X., Liu, Y., Resto Irizarry, A.M., Tang, H., and Fu, J. (2021).
922 Branching development of early post-implantation human embryonic-like tissues in 3D
923 stem cell culture. Biomaterials *275*, 120898.
924 Enders, A.C., Hendrickx, A.G., and Schlafke, S. (1983). Implantation in the rhesus
925 monkey: initial penetration of endometrium. The American journal of anatomy *167*, 275-
926 298.
927 Enders, A.C., Schlafke, S., and Hendrickx, A.G. (1986). Differentiation of the embryonic
928 disc, amnion, and yolk sac in the rhesus monkey. The American journal of anatomy
929 *177*, 161-185.
930 Granja, J.M., Klemm, S., McGinnis, L.M., Kathiria, A.S., Mezger, A., Corces, M.R.,
931 Parks, B., Gars, E., Liedtke, M., Zheng, G.X.Y.*, et al.* (2019). Single-cell multiomic
932 analysis identifies regulatory programs in mixed-phenotype acute leukemia. Nature
933 biotechnology *37*, 1458-1465.
934 Gunne-Braden, A., Sullivan, A., Gharibi, B., Sheriff, R.S.M., Maity, A., Wang, Y.F.,
935 Edwards, A., Jiang, M., Howell, M., Goldstone, R.*, et al.* (2020). GATA3 Mediates a
936 Fast, Irreversible Commitment to BMP4-Driven Differentiation in Human Embryonic
937 Stem Cells. Cell stem cell *26*, 693-706 e699.
938 Hamed, M.M., Taniguchi, K., and Duncan, M.C. (2023). Monitoring Effects of Membrane
939 Traffic Via Changes in Cell Polarity and Morphogenesis in Three-Dimensional Human
940 Pluripotent Stem Cell Cysts. Methods in molecular biology *2557*, 83-98.
941 Kinoshita, M., and Smith, A. (2018). Pluripotency Deconstructed. Development, growth
942 & differentiation *60*, 44-52.

943 Lacoste, A., Berenshteyn, F., and Brivanlou, A.H. (2009). An efficient and reversible
944 transposable system for gene delivery and lineage-specific differentiation in human
945 embryonic stem cells. Cell stem cell *5*, 332-342.
946 Livak, K.J., and Schmittgen, T.D. (2001). Analysis of relative gene expression data
947 using real-time quantitative PCR and the 2(-Delta Delta C(T)) Method. Methods *25*, 402-
948 408.
949 Miki, T., Lehmann, T., Cai, H., Stolz, D.B., and Strom, S.C. (2005). Stem cell
950 characteristics of amniotic epithelial cells. Stem cells *23*, 1549-1559.
951 Miki, T., and Strom, S.C. (2006). Amnion-derived pluripotent/multipotent stem cells.
952 Stem Cell Rev *2*, 133-142.
953 Nakamura, T., Fujiwara, K., Saitou, M., and Tsukiyama, T. (2021). Non-human primates
954 as a model for human development. Stem cell reports *16*, 1093-1103.
955 Nakamura, T., Okamoto, I., Sasaki, K., Yabuta, Y., Iwatani, C., Tsuchiya, H., Seita, Y.,
956 Nakamura, S., Yamamoto, T., and Saitou, M. (2016). A developmental coordinate of
957 pluripotency among mice, monkeys and humans. Nature *537*, 57-62.
958 Nakamura, T., Yabuta, Y., Okamoto, I., Sasaki, K., Iwatani, C., Tsuchiya, H., and
959 Saitou, M. (2017). Single-cell transcriptome of early embryos and cultured embryonic
960 stem cells of cynomolgus monkeys. Scientific data *4*, 170067.
961 Nasr Esfahani, S., Shao, Y., Resto Irizarry, A.M., Li, Z., Xue, X., Gumucio, D.L., and Fu,
962 J. (2019). Microengineered human amniotic ectoderm tissue array for high-content
963 developmental phenotyping. Biomaterials *216*, 119244.

964 Rothstein, M., and Simoes-Costa, M. (2020). Heterodimerization of TFAP2 pioneer
965 factors drives epigenomic remodeling during neural crest specification. Genome Res
966 *30*, 35-48.
967 Sasaki, K., Nakamura, T., Okamoto, I., Yabuta, Y., Iwatani, C., Tsuchiya, H., Seita, Y.,
968 Nakamura, S., Shiraki, N., Takakuwa, T.*, et al.* (2016). The Germ Cell Fate of
969 Cynomolgus Monkeys Is Specified in the Nascent Amnion. Developmental cell *39*, 169-
970 185.
971 Shahbazi, M.N., Scialdone, A., Skorupska, N., Weberling, A., Recher, G., Zhu, M.,
972 Jedrusik, A., Devito, L.G., Noli, L., Macaulay, I.C.*, et al.* (2017). Pluripotent state
973 transitions coordinate morphogenesis in mouse and human embryos. Nature *552*, 239-
974 243.
975 Shahbazi, M.N., and Zernicka-Goetz, M. (2018). Deconstructing and reconstructing the
976 mouse and human early embryo. Nature cell biology.
977 Shao, Y., and Fu, J. (2022). Engineering multiscale structural orders for high-fidelity
978 embryoids and organoids. Cell stem cell *29*, 722-743.
979 Shao, Y., Taniguchi, K., Gurdziel, K., Townshend, R.F., Xue, X., Yong, K.M.A., Sang, J.,
980 Spence, J.R., Gumucio, D.L., and Fu, J. (2017a). Self-organized amniogenesis by
981 human pluripotent stem cells in a biomimetic implantation-like niche. Nature materials
982 *16*, 419-425.
983 Shao, Y., Taniguchi, K., Townshend, R.F., Miki, T., Gumucio, D.L., and Fu, J. (2017b).
984 A pluripotent stem cell-based model for post-implantation human amniotic sac
985 development. Nature communications *8*, 208.

986 Smith, A. (2017). Formative pluripotency: the executive phase in a developmental
987 continuum. Development *144*, 365-373.
988 Takaku, M., Grimm, S.A., Shimbo, T., Perera, L., Menafra, R., Stunnenberg, H.G.,
989 Archer, T.K., Machida, S., Kurumizaka, H., and Wade, P.A. (2016). GATA3-dependent
990 cellular reprogramming requires activation-domain dependent recruitment of a
991 chromatin remodeler. Genome Biol *17*, 36.
992 Tanaka, H., Takizawa, Y., Takaku, M., Kato, D., Kumagawa, Y., Grimm, S.A., Wade,
993 P.A., and Kurumizaka, H. (2020). Interaction of the pioneer transcription factor GATA3
994 with nucleosomes. Nature communications *11*, 4136.
995 Taniguchi, K., Heemskerk, I., and Gumucio, D.L. (2019). Opening the black box: Stem
996 cell-based modeling of human post-implantation development. The Journal of cell
997 biology *218*, 410-421.
998 Taniguchi, K., Shao, Y., Townshend, R.F., Cortez, C.L., Harris, C.E., Meshinchi, S.,
999 Kalantry, S., Fu, J., O'Shea, K.S., and Gumucio, D.L. (2017). An apicosome initiates
1000 self-organizing morphogenesis of human pluripotent stem cells. The Journal of cell
1001 biology *216*, 3981-3990.
1002 Taniguchi, K., Shao, Y., Townshend, R.F., Tsai, Y.H., DeLong, C.J., Lopez, S.A.,
1003 Gayen, S., Freddo, A.M., Chue, D.J., Thomas, D.J.*, et al.* (2015). Lumen Formation Is
1004 an Intrinsic Property of Isolated Human Pluripotent Stem Cells. Stem cell reports *5*, 954-
1005 962.
1006 Townshend, R.F., Shao, Y., Wang, S., Cortez, C.L., Esfahani, S.N., Spence, J.R.,
1007 O'Shea, K.S., Fu, J., Gumucio, D.L., and Taniguchi, K. (2020). Effect of Cell Spreading

1008 on Rosette Formation by Human Pluripotent Stem Cell-Derived Neural Progenitor Cells.
1009 Front Cell Dev Biol *8*, 588941.
1010 Tyser, R.C.V., Mahammadov, E., Nakanoh, S., Vallier, L., Scialdone, A., and Srinivas,
1011 S. (2021). Single-cell transcriptomic characterization of a gastrulating human embryo.
1012 Nature *600*, 285-289.
1013 Van Otterloo, E., Milanda, I., Pike, H., Thompson, J.A., Li, H., Jones, K.L., and Williams,
1014 T. (2022). AP-2alpha and AP-2beta cooperatively function in the craniofacial surface
1015 ectoderm to regulate chromatin and gene expression dynamics during facial
1016 development. eLife *11*.
1017 Vincentz, J.W., Casasnovas, J.J., Barnes, R.M., Que, J., Clouthier, D.E., Wang, J., and
1018 Firulli, A.B. (2016). Exclusion of Dlx5/6 expression from the distal-most mandibular
1019 arches enables BMP-mediated specification of the distal cap. Proceedings of the
1020 National Academy of Sciences of the United States of America *113*, 7563-7568.
1021 Wang, S., Lin, C.W., Carleton, A.E., Cortez, C.L., Johnson, C., Taniguchi, L.E.,
1022 Sekulovski, N., Townshend, R.F., Basrur, V., Nesvizhskii, A.I.*, et al.* (2021). Spatially
1023 resolved cell polarity proteomics of a human epiblast model. Sci Adv *7*.
1024 Yang, R., Goedel, A., Kang, Y., Si, C., Chu, C., Zheng, Y., Chen, Z., Gruber, P.J., Xiao,
1025 Y., Zhou, C.*, et al.* (2021). Amnion signals are essential for mesoderm formation in
1026 primates. Nature communications *12*, 5126.
1027 Zaret, K.S., and Carroll, J.S. (2011). Pioneer transcription factors: establishing
1028 competence for gene expression. Genes & development *25*, 2227-2241.

1029 Zhao, C., Reyes, A.P., Schell, J.P., Weltner, J., Ortega, N.M., Zheng, Y., Björklund,
1030 Å.K., Rossant, J., Fu, J., Petropoulos, S.*, et al.* (2021). Reprogrammed blastoids
1031 contain amnion-like cells but not trophectoderm. bioRxiv, 2021.2005.2007.442980.
1032 Zheng, Y., Xue, X., Shao, Y., Wang, S., Esfahani, S.N., Li, Z., Muncie, J.M., Lakins,
1033 J.N., Weaver, V.M., Gumucio, D.L.*, et al.* (2019). Controlled modelling of human
1034 epiblast and amnion development using stem cells. Nature *573*, 421-425.
1035 Zheng, Y., Yan, R.Z., Sun, S., Kobayashi, M., Xiang, L., Yang, R., Goedel, A., Kang, Y.,
1036 Xue, X., Esfahani, S.N.*, et al.* (2022). Single-cell analysis of embryoids reveals lineage
1037 diversification roadmaps of early human development. Cell stem cell *29*, 1402-1419
1038 e1408.

1039

Figure 1

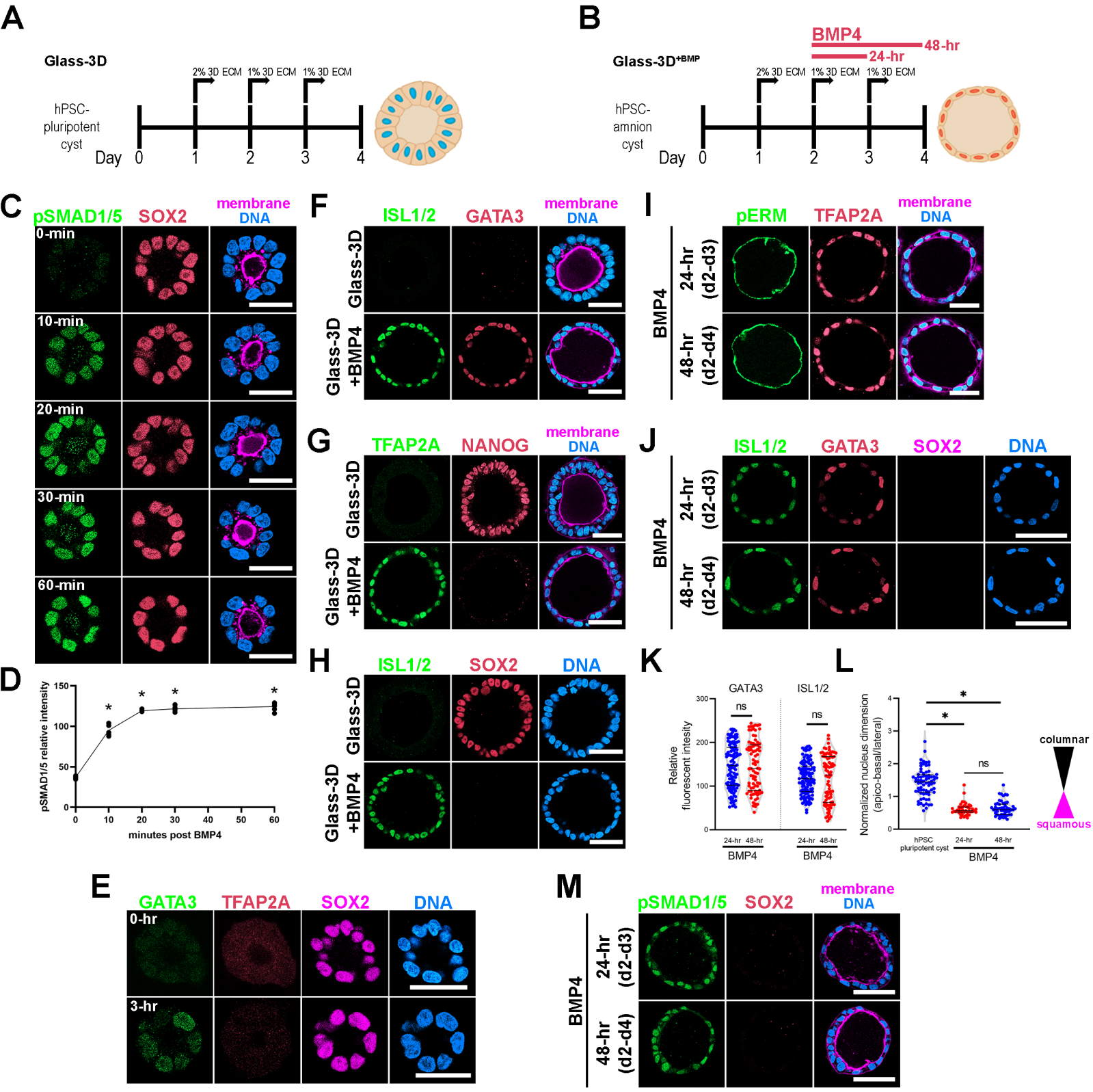
A
Glass-3D
2% 3D ECM
1% 3D ECM
1% 3D ECM
hPSC-pluripotent cyst
Day 0 1 2 3 4
B
BMP4
48-hr
24-hr
Glass-3D+BMP
2% 3D ECM
1% 3D ECM
1% 3D ECM
hPSC-amnion cyst
Day 0 1 2 3 4
C
pSMAD1/5
SOX2
membrane DNA
0-min
10-min
20-min
30-min
60-min
D
pSMAD1/5 relative intensity
minutes post BMP4
E
GATA3
TFAP2A
SOX2
DNA
0-hr
3-hr
F
ISL1/2
GATA3
membrane DNA
Glass-3D
Glass-3D +BMP4
G
TFAP2A
NANOG
membrane DNA
Glass-3D
Glass-3D +BMP4
H
ISL1/2
SOX2
DNA
Glass-3D
Glass-3D +BMP4
I
pERM
TFAP2A
membrane DNA
BMP4
24-hr (d2-d3)
48-hr (d2-d4)
J
ISL1/2
GATA3
SOX2
DNA
BMP4
24-hr (d2-d3)
48-hr (d2-d4)
K
GATA3
ISL1/2
ns
Relative fluorescent intesity
24-hr 48-hr
BMP4
L
Normalized nucleus dimension (apico-basal/lateral)
hPSC pluripotent cyst
24-hr
48-hr
BMP4
columnar
squamous
M
pSMAD1/5
SOX2
membrane DNA
BMP4
24-hr (d2-d3)
48-hr (d2-d4)

Figure 2

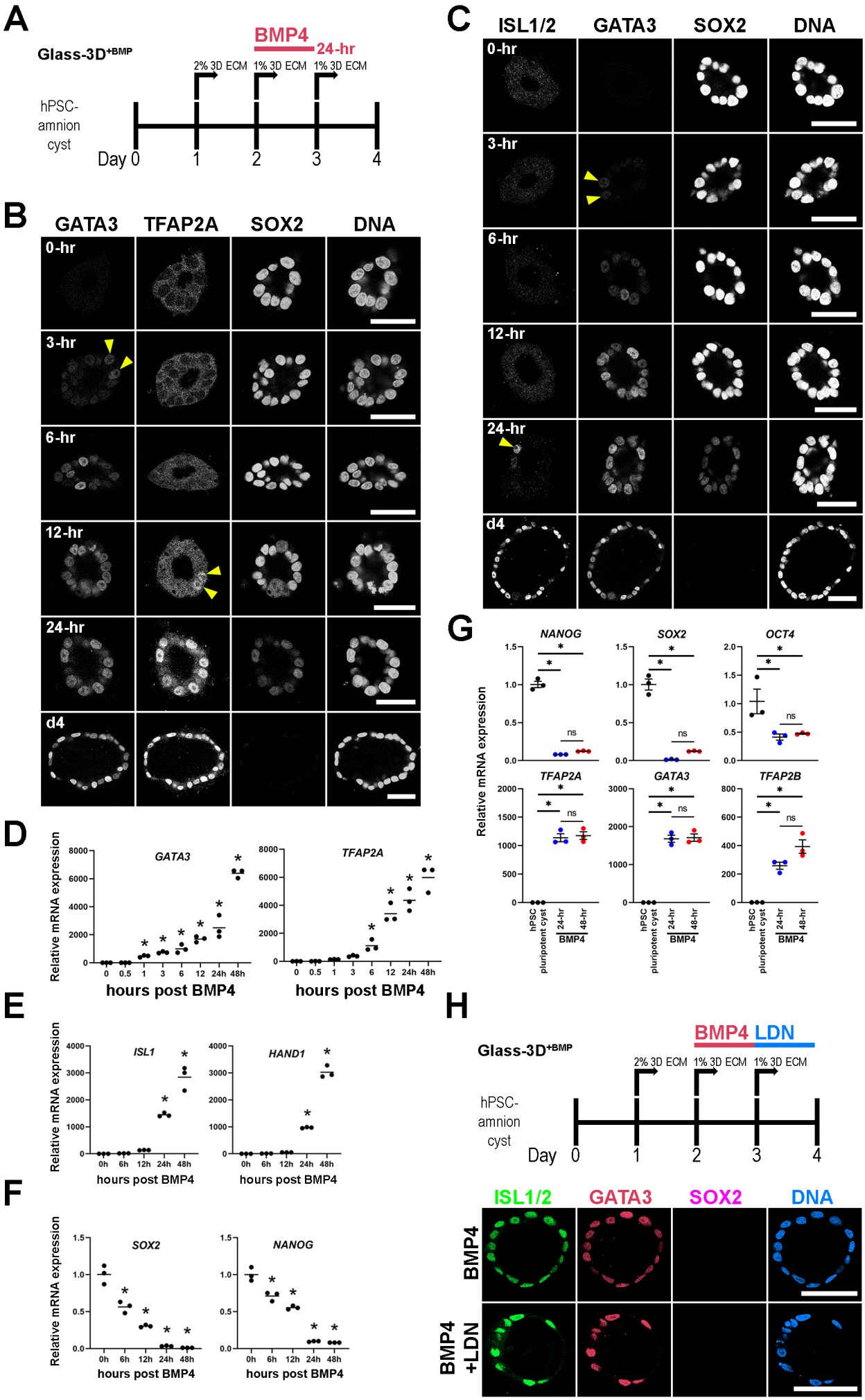
A
Glass-3D+BMP
BMP4
24-hr
2% 3D ECM
1% 3D ECM
1% 3D ECM
hPSC-amnion cyst
Day 0
1
2
3
4
B
GATA3
TFAP2A
SOX2
DNA
0-hr
3-hr
6-hr
12-hr
24-hr
d4
C
ISL1/2
GATA3
SOX2
DNA
0-hr
3-hr
6-hr
12-hr
24-hr
d4
D
GATA3
TFAP2A
Relative mRNA expression
hours post BMP4
E
ISL1
HAND1
Relative mRNA expression
hours post BMP4
F
SOX2
NANOG
Relative mRNA expression
hours post BMP4
G
NANOG
SOX2
OCT4
TFAP2A
GATA3
TFAP2B
Relative mRNA expression
hPSC
pluripotent cyst
24-hr
48-hr
BMP4
ns
H
Glass-3D+BMP
BMP4 LDN
2% 3D ECM
1% 3D ECM
1% 3D ECM
hPSC-amnion cyst
Day 0
1
2
3
4
ISL1/2
GATA3
SOX2
DNA
BMP4
BMP4 +LDN

Figure 3

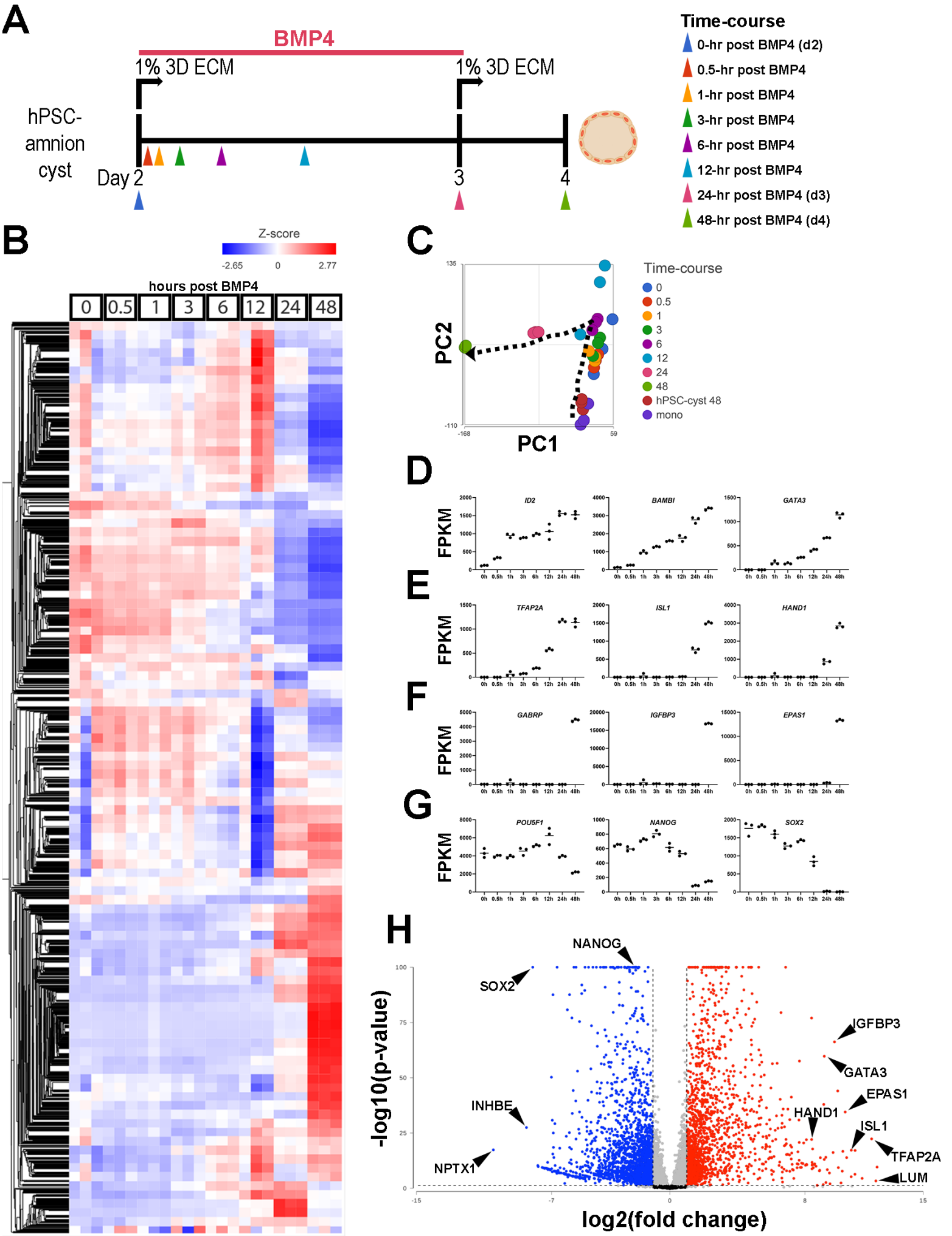
A
BMP4
1% 3D ECM
1% 3D ECM
hPSC-amnion cyst
Day 2
3
4
Time-course
0-hr post BMP4 (d2)
0.5-hr post BMP4
1-hr post BMP4
3-hr post BMP4
6-hr post BMP4
12-hr post BMP4
24-hr post BMP4 (d3)
48-hr post BMP4 (d4)
B
Z-score
-2.65
0
2.77
hours post BMP4
0
0.5
1
3
6
12
24
48
C
PC2
PC1
Time-course
0
0.5
1
3
6
12
24
48
hPSC-cyst 48
mono
D
E
F
G
FPKM
ID2
BAMBI
GATA3
TFAP2A
ISL1
HAND1
GABRP
IGFBP3
EPAS1
POU5F1
NANOG
SOX2
H
NANOG
SOX2
IGFBP3
GATA3
EPAS1
HAND1
ISL1
TFAP2A
LUM
INHBE
NPTX1
-log10(p-value)
log2(fold change)

Figure 4

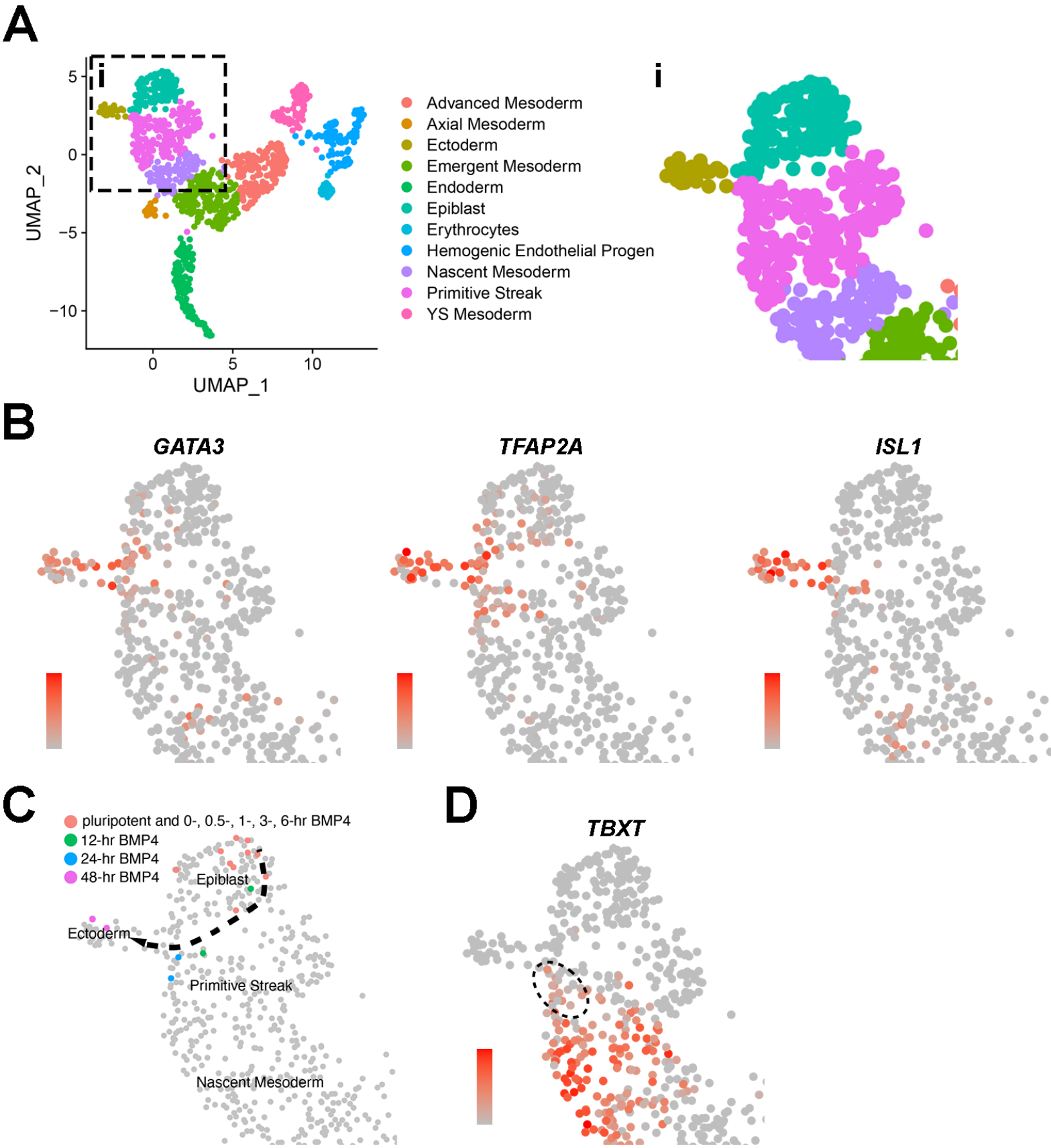
A
i
UMAP_2
UMAP_1
5
0
−5
−10
0
5
10
Advanced Mesoderm
Axial Mesoderm
Ectoderm
Emergent Mesoderm
Endoderm
Epiblast
Erythrocytes
Hemogenic Endothelial Progen
Nascent Mesoderm
Primitive Streak
YS Mesoderm
i
B
GATA3
TFAP2A
ISL1
C
pluripotent and 0-, 0.5-, 1-, 3-, 6-hr BMP4
12-hr BMP4
24-hr BMP4
48-hr BMP4
Epiblast
Ectoderm
Primitive Streak
Nascent Mesoderm
D
TBXT

Figure 5

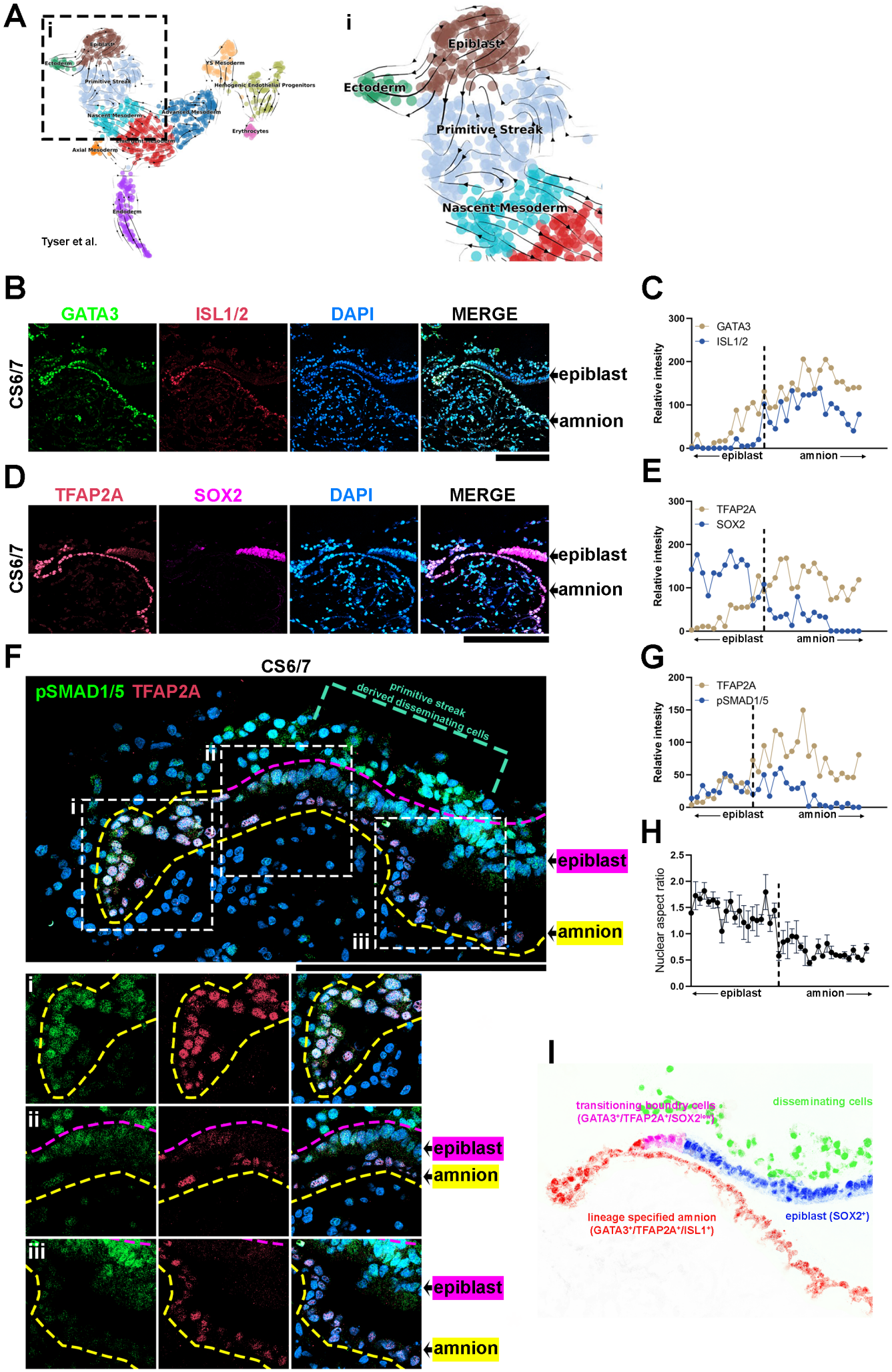
A
i
Epiblast
Ectoderm
Primitive Streak
Nascent Mesoderm
Advanced Mesoderm
YS Mesoderm
Hemogenic Endothelial Progenitors
Erythrocytes
Endoderm
Tyser et al.
Epiblast
Ectoderm
Primitive Streak
Nascent Mesoderm
B
GATA3
ISL1/2
DAPI
MERGE
CS6/7
epiblast
amnion
C
GATA3
ISL1/2
Relative intesity
epiblast
amnion
D
TFAP2A
SOX2
DAPI
MERGE
CS6/7
epiblast
amnion
E
TFAP2A
SOX2
Relative intesity
epiblast
amnion
F
CS6/7
pSMAD1/5 TFAP2A
primitive streak derived disseminating cells
ii
i
iii
epiblast
amnion
G
TFAP2A
pSMAD1/5
Relative intesity
epiblast
amnion
H
Nuclear aspect ratio
epiblast
amnion
i
ii
iii
epiblast
amnion
epiblast
amnion
I
transitioning boundry cells
(GATA3+/TFAP2A+/SOX2low)
disseminating cells
lineage specified amnion
(GATA3+/TFAP2A+/ISL1+)
epiblast (SOX2+)

Figure 6

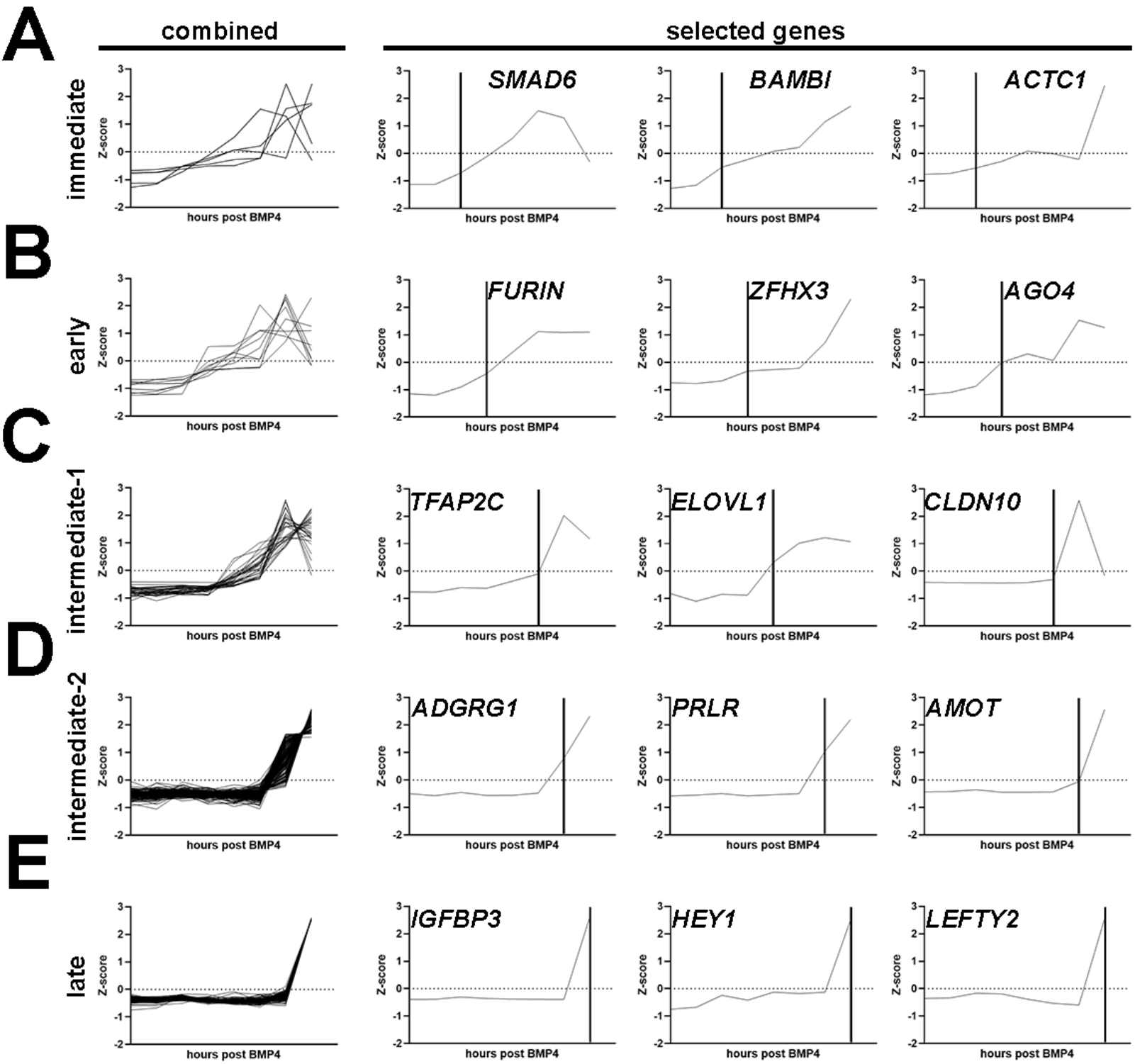
A
B
C
D
E
combined
selected genes
immediate
early
intermediate-1
intermediate-2
late
SMAD6
BAMBI
ACTC1
FURIN
ZFHX3
AGO4
TFAP2C
ELOVL1
CLDN10
ADGRG1
PRLR
AMOT
IGFBP3
HEY1
LEFTY2
Z-score
hours post BMP4

Figure 7

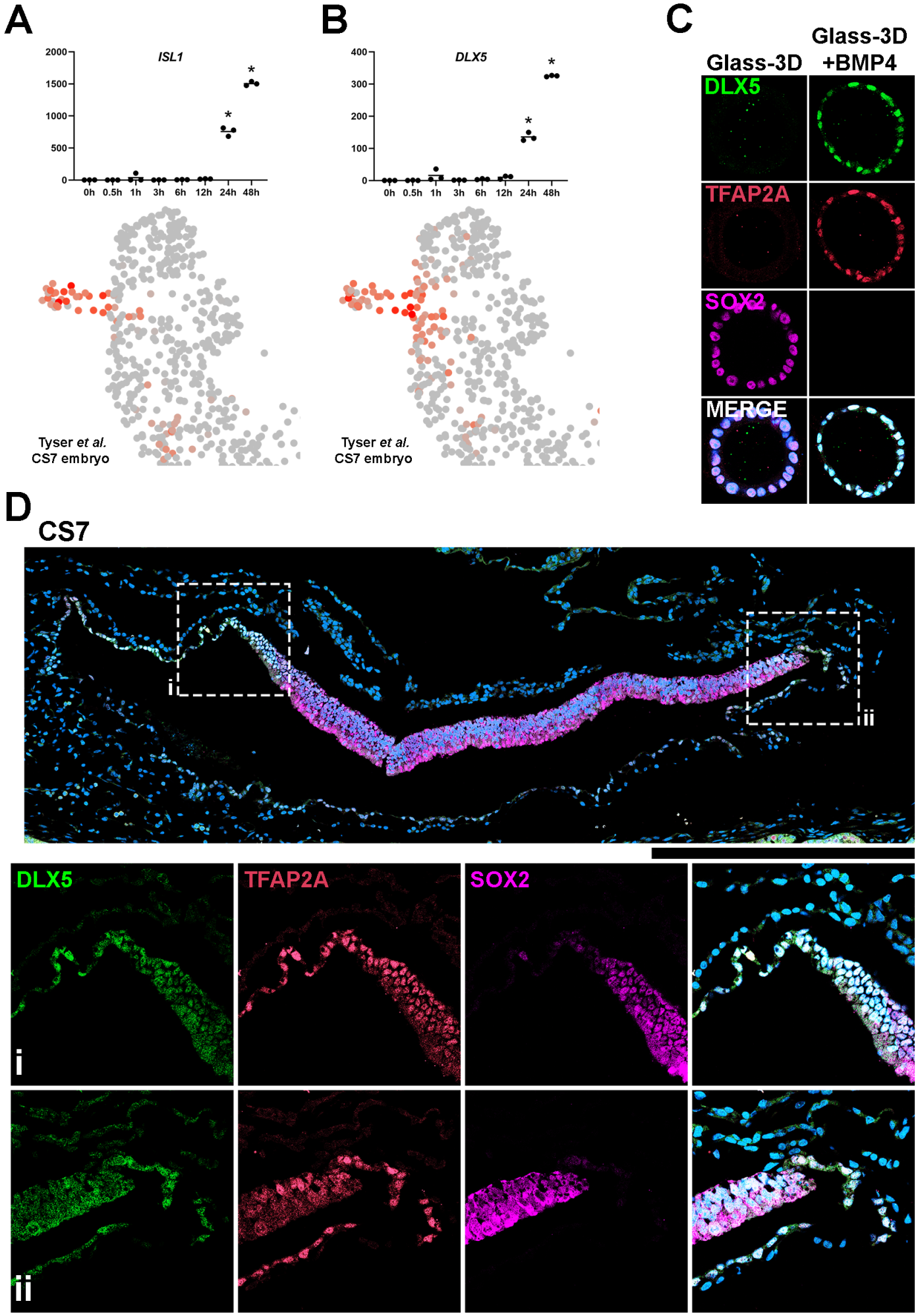
A
ISL1
2000
1500
1000
500
0
0h 0.5h 1h 3h 6h 12h 24h 48h
Tyser et al.
CS7 embryo
B
DLX5
400
300
200
100
0
0h 0.5h 1h 3h 6h 12h 24h 48h
Tyser et al.
CS7 embryo
C
Glass-3D
Glass-3D +BMP4
DLX5
TFAP2A
SOX2
MERGE
D
CS7
i
ii
DLX5
TFAP2A
SOX2
i
ii

Figure 8

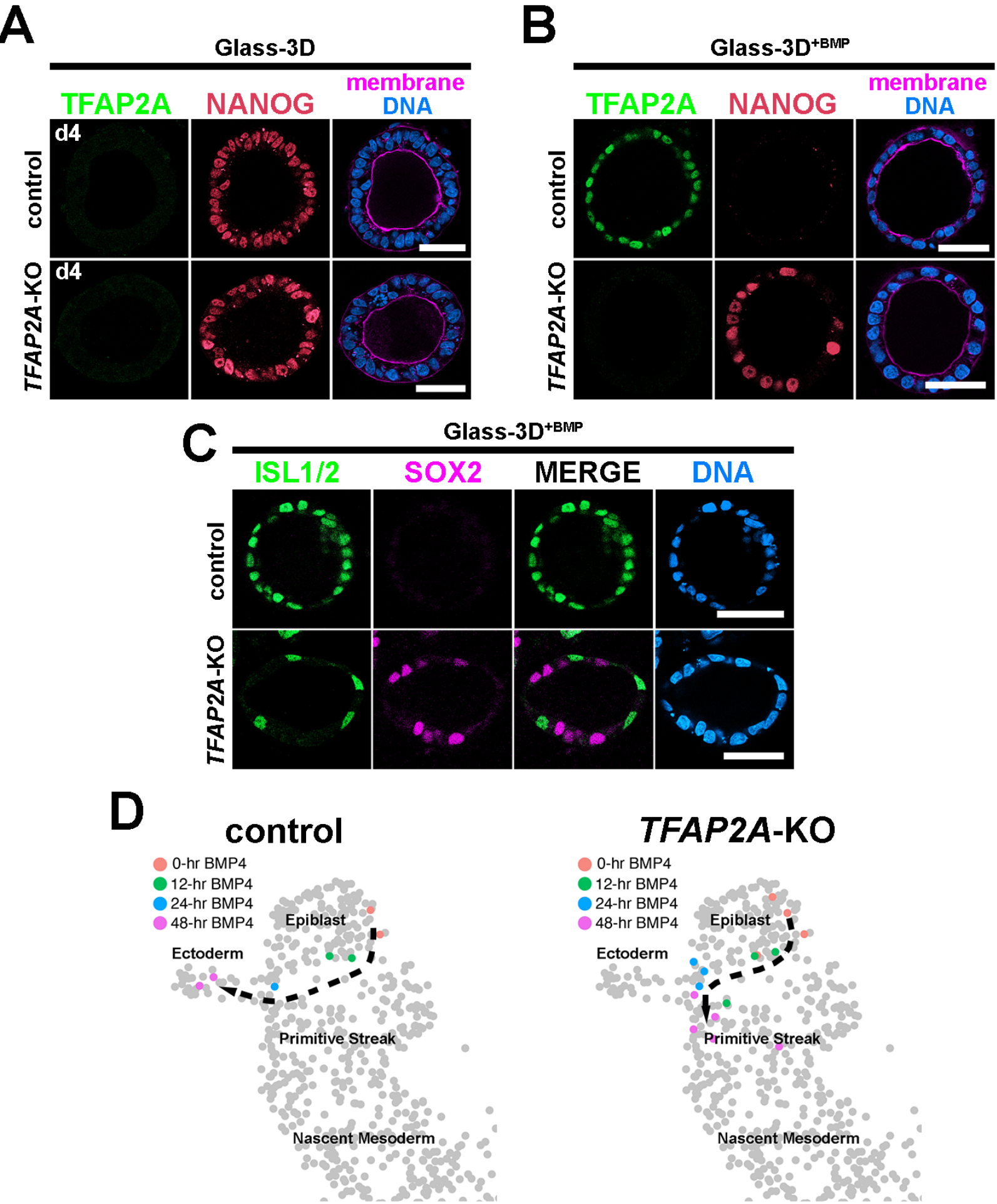
A
Glass-3D
TFAP2A
NANOG
membrane
DNA
d4
control
d4
TFAP2A-KO
B
Glass-3D+BMP
TFAP2A
NANOG
membrane
DNA
control
TFAP2A-KO
C
Glass-3D+BMP
ISL1/2
SOX2
MERGE
DNA
control
TFAP2A-KO
D
control
0-hr BMP4
12-hr BMP4
24-hr BMP4
48-hr BMP4
Epiblast
Ectoderm
Primitive Streak
Nascent Mesoderm
TFAP2A-KO
0-hr BMP4
12-hr BMP4
24-hr BMP4
48-hr BMP4
Epiblast
Ectoderm
Primitive Streak
Nascent Mesoderm